



1 **Changing pattern of ice flow and mass balance for glaciers discharging into the Larsen A and**
2 **B embayments, Antarctic Peninsula, 2011 to 2016**

3

4 Helmut Rott^{1,2*}, Wael Abdel Jaber³, Jan Wuite¹, Stefan Scheiblauer¹, Dana Floricioiu³, Jan
5 Melchior van Wessem⁴, Thomas Nagler¹, Nuno Miranda⁵, Michiel R. van den Broeke⁴

6

7 [1] ENVEO IT GmbH, Innsbruck, Austria

8 [2] Institute of Atmospheric and Cryospheric Sciences, University of Innsbruck, Innsbruck, Austria

9 [3] Institute for Remote Sensing Technology, German Aerospace Center, Oberpfaffenhofen,
10 Germany

11 [4] Institute for Marine and Atmospheric Research, Utrecht University, Utrecht, the Netherlands

12 [5] European Space Agency/ESRIN, Frascati, Italy

13 *Correspondence to: Helmut.Rott@enveo.at

14

15



16 **Abstract**

17

18 We analyzed volume change and mass balance of outlet glaciers on the northern Antarctic Peninsula
19 over the periods 2011 to 2013 and 2013 to 2016, using high resolution topographic data of the
20 bistatic interferometric radar satellite mission TanDEM-X. Complementary to the geodetic method
21 applying DEM differencing, we computed the net mass balance of the main outlet glaciers by the
22 input/output method, accounting for the difference between the surface mass balance (SMB) and the
23 discharge of ice into an ocean or ice shelf. The SMB values are based on output of the regional
24 climate model RACMO Version 2.3p2. For studying glacier flow and retrieving ice discharge we
25 generated time series of ice velocity from data of different satellite radar sensor, with radar images
26 of the satellites TerraSAR-X and TanDEM-X as main source. The study area comprises tributaries
27 to the Larsen-A, Larsen Inlet, and Prince-Gustav-Channel embayments (region A), the glaciers
28 calving into Larsen B embayment (region B), and the glaciers draining into the remnant part of
29 Larsen B ice shelf in SCAR Inlet (region C). The glaciers of region A, where the buttressing ice
30 shelf disintegrated in 1995, and of region B (ice shelf break-up in 2002) show continuing losses in
31 ice mass, with significant reduction of losses after 2013. The mass balance numbers for grounded
32 glacier area of the region A are $B_n = -3.98 \pm 0.33 \text{ Gt a}^{-1}$ during 2011 to 2013 and $B_n = -2.38 \pm 0.18$
33 Gt a^{-1} during 2013 to 2016. The corresponding numbers for region B are $B_n = -5.75 \pm 0.45 \text{ Gt a}^{-1}$
34 and $B_n = -2.32 \pm 0.25 \text{ Gt a}^{-1}$. The mass losses in region C during the two periods were modest, $B_n =$
35 $-0.54 \pm 0.38 \text{ Gt a}^{-1}$, respectively $B_n = -0.58 \pm 0.25 \text{ Gt a}^{-1}$. The main share in the overall mass losses
36 of the region were contributed by two glaciers: Drygalski Glacier contributing 61 % to the mass
37 deficit of region A, and Hektoría and Green glaciers accounting for 67 % to the mass deficit of
38 region B. Hektoría and Green glaciers accelerated significantly in 2010/2011, triggering elevation
39 losses up to 19.5 m a^{-1} on the lower terminus and a rate of mass depletion of 3.88 Gt a^{-1} during the
40 period 2011 to 2013. Slowdown of calving velocities and reduced calving fluxes in 2013 to 2016
41 coincided with years when the sea ice cover in front of the glaciers persisted during summer.

42

43



44 1. Introduction

45 The disintegration of the ice shelves in Prince-Gustav-Channel and the Larsen A embayment in
46 January 1995 (Rott et al., 1996) and the break-up of the northern and central sections of Larsen B
47 embayment in March 2002 (Rack and Rott, 2004; Glasser and Scambos, 2008) triggered near-
48 immediate acceleration of the outlet glaciers previously feeding the ice shelves, resulting in major
49 mass losses due to increased ice discharge (Rott et al., 2002; De Angelis and Skvarca, 2003;
50 Scambos et al., 2004; Scambos et al., 2011). Precise, spatially detailed data on flow dynamics and
51 mass balance of these glaciers since ice-shelf disintegration are essential for understanding the
52 complex glacier response to the loss of ice shelf buttressing, as well as to learn about processes
53 controlling the adaptation to new boundary conditions. Furthermore, due to the complex topography
54 of this region, spatially detailed data on glacier surface elevation change and mass balance are the
55 key for reducing the uncertainty of northern Antarctic Peninsula (API) contributions to sea level
56 rise.

57 Several studies dealt with mass balance, acceleration and thinning of glaciers after disintegration of
58 the Larsen A and B ice shelves, with the majority focusing on glaciers of the Larsen B embayment.
59 A complete, detailed analysis of changes in ice mass was performed by Scambos et al. (2014) for 33
60 glacier basins covering the API mainland and adjoining islands north of 66°S, using a combination
61 of digital elevation model (DEM) differencing from optical stereo satellite images and repeat-track
62 laser altimetry from the Ice, Cloud, and Land Elevation Satellite (ICESat). The DEM difference
63 pairs cover the periods 2001-2006, 2003-2008, and 2004-2010 for different sections of the study
64 area, and are integrated with ICESat data of the years 2003 to 2008. A detailed analysis of surface
65 elevation change and mass depletion for API outlet glaciers draining into the Larsen-A, Larsen
66 Inlet, and Prince-Gustav-Channel (PGC) embayments during 2011 to 2013 was reported by Rott et
67 al. (2014), based on topographic data of the TanDEM-X/TerraSAR-X satellite formation. With an
68 annual loss in ice mass of $4.21 \pm 0.37 \text{ Gt a}^{-1}$ during 2011-2013 these glaciers were still largely out
69 of balance, although the loss rate during this period was diminished by 27% compared to the loss
70 rate reported by Scambos et al. (2014) for 2001 to 2008. Studies on frontal retreat, ice velocities,
71 and ice discharge, based on remote sensing data of the period 1992 to 2014, are reported by Seehaus
72 et al. (2015) for the Dinsmoor–Bombardier–Edgeworth glacier system previously feeding the
73 Larsen A ice shelf and by Seehaus et al. (2016) for glaciers of Sjögren Inlet previously feeding the
74 PGC ice shelf.

75 As observed previously for Larsen A (Rott et al., 2002), the major outlet glaciers to the Larsen B
76 embayment started to accelerate and get thinner immediately after the collapse of the ice shelf
77 (Rignot et al., 2004; Scambos et al., 2004; De Rydt et al., 2015). The patterns of acceleration,



78 thinning and change of frontal position have been variable in time and space. After strong
79 acceleration during the first years, some of the main glaciers slowed down significantly after 2007,
80 resulting in major decrease of calving fluxes. Other glaciers continued to show widespread
81 fluctuations in velocity, with periods of major frontal retreat alternating with stationary positions or
82 intermittent frontal advance (Wuite et al., 2015). The remnant section of Larsen B ice shelf in
83 SCAR inlet started to accelerate soon after the central and northern sections of the ice shelf broke
84 away, triggering modest acceleration of the main glaciers flowing into the SCAR inlet ice shelf
85 (Wuite et al., 2015; Khazendar et al., 2015).

86 Several publications reported on ice export and mass balance of Larsen-B glaciers. Shuman et al.
87 (2011) derived surface elevation change from optical stereo satellite imagery and laser altimetry of
88 ICESat and the airborne Airborne Topographic Mapper (ATM) of NASA's IceBridge program. For
89 the period 2001 to 2006 they report a combined rate of mass losses of $8.4 \pm 1.7 \text{ Gt a}^{-1}$ for the
90 glaciers discharging into Larsen B embayment and SCAR Inlet, excluding ice lost by frontal retreat.
91 ICESat and ATM altimetry measurements spanning 2002–2009 show for lower Crane Glacier a
92 period of very rapid drawdown between September 2004 and September 2005, bounded by periods
93 of more moderate rates of surface lowering (Scambos et al., 2011). Rott et al. (2011) derived
94 velocities and ice discharge of the nine main Larsen B glaciers in pre-collapse state (1995 and 1999)
95 and for 2008–2009, estimating the mass imbalance of these glaciers in 2008 at $4.34 \pm 1.64 \text{ Gt a}^{-1}$.
96 Berthier et al. (2012) report a mass loss rate of $9.04 \pm 2.01 \text{ Gt a}^{-1}$ for Larsen B glaciers, excluding
97 SCAR inlet, for the period 2006 to 2010/2011, based on altimetry and optical stereo imagery.
98 Scambos et al. (2014) analysed changes in ice mass from ICESat data spanning September 2003 to
99 March 2008 and stereo image DEMs spanning 2001/2002 to 2006. They report a combined rate of
100 mass losses of 7.9 Gt a^{-1} for the tributaries of the Larsen B embayment and of 1.4 Gt a^{-1} for the
101 tributaries to SCAR Inlet ice shelf. Wuite et al. (2015) report for main outlet glaciers strongly
102 reduced calving fluxes during the period 2010 to 2013 compared to the first few years after ice shelf
103 collapse.

104 We use high resolution data of surface topography derived from synthetic aperture radar
105 interferometry (InSAR) satellite measurements for retrieving changes in glacier volume and
106 estimating glacier mass balance over well-defined epochs for API outlet glaciers along the Weddell
107 Coast between PGC and Jason Peninsula. In addition, we generate ice velocity maps to study the
108 temporal evolution of ice motion and derive the ice discharge for the major glacier drainage basins.
109 We compute the mass balance also by means of the input-output method (IOM), quantifying the
110 difference between glacier surface mass balance (SMB) and the discharge of ice into the ocean or
111 across the grounding line to an ice shelf. The SMB estimates are obtained from output of the



112 regional atmospheric climate model RACMO Version 2.3p2 at grid size of ~ 5.5 km (van Wessem
113 et al., 2016; 2017).

114 Volume change and mass balance of glaciers discharging into the PGC, Larsen Inlet and Larsen A
115 embayments were derived by Rott et al. (2014) for the period 2011 to 2013, applying TanDEM-X
116 DEM differencing. Here we extend the observation period for the same glacier basins by covering
117 the time span 2013 to 2016. Furthermore, we present time series of surface velocity starting in
118 1993/1995 in order to relate the recent flow behavior to pre-collapse conditions.

119 For glaciers of the Larsen-B embayment we generated maps of surface elevation change by
120 TanDEM-X DEM differencing for the periods 2011 to 2013 and 2013 to 2016. From these maps we
121 derived mass changes at the scale of individual glacier drainage basins. In addition, we obtained
122 mass balance estimates for the eight main glaciers by the input/output method and compare the
123 results of the two independent methods. A detailed analysis of surface velocities of Larsen B
124 glaciers for the period 1995 to 2013 was presented by Wuite et al. (2015). We extend the time series
125 to cover glacier velocities up to 2016.

126 These data sets disclose large temporal and spatial variability in ice flow and surface elevation
127 change between different glacier basins and show ongoing loss of grounded ice. This provides a
128 valuable basis for studying factors responsible for instability and downwasting of glaciers and for
129 exploring possible mechanisms of adaptation to new boundary conditions.

130 **2. Data and methods**

131 **2.1 DEM differencing using TanDEM-X interferometric SAR data**

132 The study is based on remote sensing data from various satellite missions. We applied DEM
133 differencing using interferometric SAR data (InSAR) of the TanDEM-X mission to map the surface
134 elevation change and retrieve the mass balance for 24 catchments on the API east coast between
135 PGC and Jason Peninsula (Supplement, Table S1). Large glaciers are retained as single catchments
136 whereas smaller glaciers and glaciers that used to share the same outlet are grouped together. For
137 separation of glacier drainage basins inland of the frontal areas the glacier outlines of the
138 Glaciology Group, University of Swansea, are used which are available at the GLIMS data base
139 (Cook et al., 2014). We updated the glacier fronts for several dates of the study period using
140 TerraSAR-X, TanDEM-X and Landsat-8 images. Catchment outlines and frontal positions in 2011,
141 2013 and 2016 are plotted in a Landsat image of 2016-10-29 (Supplement, Figures S1 and S2).

142 The TanDEM-X mission (TDM) employs a bi-static interferometric configuration of the two
143 satellites TerraSAR-X and TanDEM-X flying in close formation (Krieger et al., 2013). The two
144 satellites form together a single-pass synthetic aperture radar (SAR) interferometer, enabling the



145 acquisition of highly accurate cross-track interferograms that are not affected by temporal
146 decorrelation and variations in atmospheric phase delay. The main objective of the mission is the
147 acquisition of a global DEM with high accuracy. The 90 % relative point-to-point height accuracy
148 for moderate terrain is ± 2 m at 12 m posting (Rossi et al., 2012; Rizzoli et al., 2012). Higher relative
149 vertical accuracy can be achieved for measuring elevation change over time.

150 Our analysis of elevation change is based on DEMs derived from interferograms acquired by the
151 TanDEM-X mission in mid-2011, -2013 and -2016. SAR data takes from descending satellite orbits,
152 acquired in 2013 and 2016, cover the API east coast glaciers between 64° S and the Jason
153 Peninsula, as well as parts of the west coast glaciers (Supplement, Figure S3). For 2011 we
154 processed data takes covering the Larsen B glaciers. Over the Larsen A glaciers TDM data from
155 2011 and 2013 had been processed in an earlier study to derive surface elevation change (SEC). The
156 mid-beam incidence angle of the various tracks varies between 36.1 and 45.6 degrees. The height of
157 ambiguity (HoA, the elevation difference corresponding to a phase cycle of 2π) varies between 20.6
158 m and 68.9 m, providing good sensitivity to elevation (Rott, 2009) (Supplement, Table S2). Only
159 track A has larger HoA and thus less height sensitivity; this track extends along the west coast and
160 covers only a very small section of study glaciers along the Weddell Coast.

161 We used the operational Integrated TanDEM-X Processor (ITP) of the German Aerospace Center
162 (DLR) to process the raw bistatic SAR data of the individual tracks into so-called Raw DEMs
163 (Rossi et al., 2012; Abdel Jaber et al., 2016). In the production line for the global DEM, which also
164 uses the ITP Processor, Raw DEMs are intermediate products before DEM mosaicking. An option
165 recently added to the ITP foresees the use of reference DEMs to support Raw DEM processing
166 (Lachaise and Fritz, 2016). We applied this option for generating the Raw DEMs, subtracting the
167 phase of the simulated reference DEM from the interferometric phase of the corresponding scene.
168 The recently released TanDEM-X global DEM with a posting of 0.4 arcsec was used as the main
169 source for the reference DEM. Although the relative elevation in output is not related to the
170 reference DEM, the presence of inconsistencies in the reference DEM may lead to artefacts in the
171 output DEM. Therefore some preparatory editing was performed: unreliable values were removed
172 based on the provided consistency mask of the global DEM and visual analysis and were substituted
173 by data of the Antarctic Peninsula DEM of Cook et al. (2012). The phase difference image, which
174 has a much lower fringe frequency, is unwrapped and summed up with the simulated phase image.
175 This option provides a robust phase unwrapping performance for compiling the individual DEMs.
176 By subtracting the two DEMs and accounting for the appropriate time span we obtain a surface
177 elevation rate of change map, with horizontal posting at about 12 m x 12 m.

178 For estimating the uncertainty of the TanDEM SEC maps we use a fully independent data set



179 acquired during NASA IceBridge campaigns that became available after the production of the TDM
180 SEC maps had been completed. Surface elevation rate of change data (dh/dt, product code
181 IDHDT4) derived from Airborne Topographic Mapper (ATM) swathes, acquired on 2011-11-14 and
182 2016-11-10, cover longitudinal profiles on six of our study glaciers (Studinger, 2014, updated
183 2017). Each IDHDT4 data record corresponds to an area where two ATM lidar swathes have co-
184 located measurements. The IDHDT4 data are provided as discrete points representing 250 m x 250
185 m surface area and are posted at about 80 m along-track spacing. We compare mean values of cells
186 comprising 7 x 7 TDM dh/dt pixels (12 m x 12 m pixel size) with the corresponding IDHDT4
187 points. Even though the start and end dates of the TDM and ATM data sets differ by a few months,
188 the agreement in dh/dt is very good. The root mean square differences (RMSD) of the data points
189 range from 0.14 m a⁻¹ to 0.35 m a⁻¹ for the different glaciers, and the mean difference of the ATM –
190 TDM data sets is dh/dt = -0.08 m a⁻¹. For the error analysis we assume that the differences result
191 from uncertainties in both data sets. The resulting RMSE for the TDM dh/dt cells is 0.20 m a⁻¹ over
192 the five year time span, and 0.39 m a⁻¹ and 0.58 m a⁻¹ for the three and two year time span,
193 respectively.

194 The agreement between the lidar and radar dh/dt data indicates that radar penetration is not an issue
195 for deriving elevation change from the SAR based DEMs of this study. This can be attributed to the
196 close agreement of the view angles in the corresponding SAR repeat data, acquired from the same
197 orbit track and beam, and to the consistency of radar propagation properties in the snow and firn
198 bodies. The latter point follows from the similarity of the backscatter coefficients of the
199 corresponding scenes, with differences between the two dates staying below 1 dB. The radar
200 backscatter coefficient can be used as indicator on stability in the structure and radar propagation
201 properties of a snow/ice medium which determine the signal penetration and the offset of the
202 scattering phase centre versus the surface (Rizzoli et al., 2017). The TSX and TDM SAR
203 backscatter images have high radiometric accuracy (absolute radiometric accuracy 0.7 dB, relative
204 radiometric accuracy 0.3 dB), well suitable for quantifying temporal changes in backscatter
205 (Schwerdt et al., 2010; Walter Antony et al., 2016).

206 The main outlet glaciers of the study area arise from the plateaus along the central API ice divide.
207 The plateaus stretch across elevations between about 1500 and 2000 m a.s.l. A steep escarpment,
208 dropping about 500 m in elevation, separates the plateau from the individual glacier streams and
209 cirques. The high resolution SEC maps, shown in Figures 1, 5, and 6, cover the areas below the
210 escarpment excluding parts of the steep rock- and ice- covered slopes along the glacier streams.
211 These gaps are due to the particular SAR observation geometry, with slopes facing towards the
212 illuminating radar beam appearing compressed (foreshortening) or being affected by superposition



213 of dual or multiple radar signals (layover) (Rott, 2009). On areas with gentle topography and on
214 slopes facing away from the radar beam (back-slopes) the surface elevation and its change can be
215 derived from the interferometric SAR images. In order to fill the gaps in areas of foreshortening and
216 layover, we checked topographic change on back-slopes. The TDM data set includes SEC data for
217 38 individual sections on back-slopes with mean slope angles ≥ 20 degrees, covering a total area of
218 787 km^2 . The mean dh/dt value of these slopes is -0.054 m a^{-1} . The satellite derived velocity maps
219 show surface velocities $< 0.02 \text{ m d}^{-1}$ anywhere on the slope areas, indicating that dynamic effects are
220 insignificant for mass turnover. This explains the observed stability of surface topography.

221 There are some gaps in the SEC maps also on the plateau above the escarpment. The TDM SEC
222 analysis covers substantial parts (all together 2013 km^2) of the ice plateaus between 1500 m and
223 2000 m, the mean value dh/dt is -0.012 m a^{-1} . No distinct spatial pattern is evident. Considering the
224 small change of surface elevation in the available data samples of the ice plateau and on the slopes,
225 we assume stationary conditions for the unsurveyed slopes and the central ice plateau. For
226 estimation of uncertainty we assume for these areas a bulk uncertainty $dh/dt = \pm 0.10 \text{ m a}^{-1}$ for the
227 error budget of elevation change derived from DEMs spanning three years and $dh/dt = \pm 0.15 \text{ m a}^{-1}$
228 for DEMs spanning two years.

229 **2.2 Ice velocity maps and calving fluxes**

230 We generated maps of glacier surface velocity for several dates of the study period from radar
231 satellite images, extending the available velocity time series up to 2016. The main data base for the
232 recent velocity maps are repeat-pass SAR images of the satellites TerraSAR-X and TanDEM-X.
233 Gaps in these maps, primarily in the slowly moving interior, are filled with velocities derived from
234 SAR images of Sentinel-1 (S1) and of the Phased Array L-band SAR (PALSAR) on ALOS. We
235 applied offset tracking for deriving two-dimensional surface displacements in radar geometry and
236 projected these onto the glaciers surfaces defined by the ASTER-based Antarctic Peninsula digital
237 elevation model (API-DEM) of Cook et al. (2012). The velocity data set comprises the three
238 components of the surface velocity vector in Antarctic polar stereographic projection resampled to a
239 50 m grid.

240 The TerraSAR-X/TanDEM-X velocity maps are based on SAR strip map mode images of 11-day
241 repeat-pass orbits, using data spanning one or two repeat cycles. Due to the high spatial resolution
242 of the images (3.3 m along the flight track and 1.2 m in radar line-of-sight) velocity gradients are
243 well resolved. Regarding S1 we use single look complex (SLC) Level 1 products acquired in
244 Interferometric Wide (IW) swath mode, with nominal spatial resolution $20 \text{ m} \times 5 \text{ m}$ (Torres et al.
245 2012; Nagler et al., 2015). Images of the Sentinel-1A satellite at 12-day repeat cycle cover the study



246 region since December 2014. Since September 2016 the area is also covered by the Sentinel-1B
247 satellite, providing a combined S1 data set with 6-day repeat coverage.

248 Wuite et al. (2015) estimate the uncertainty of velocity magnitude derived from TerraSAR-X 11-day
249 repeat pass images at $\pm 0.05 \text{ m d}^{-1}$. In order to check the impact of combining different ice velocity
250 products, we compared TerraSAR-X/TanDEM-X velocity maps of the study area, resampled to 200
251 m, with S1 velocity maps using data sets with a maximum time difference of 10 days. The overall
252 mean bias (S1 – TerraSAR-X/TanDEM-X) between the two data sets (sample 570,000 points) is
253 0.011 m d^{-1} for velocity component V_e (easting) and -0.002 m d^{-1} for V_n (northing), the RMSD is
254 0.175 m d^{-1} for V_e and 0.207 m d^{-1} for V_n . The good agreement of the mean velocity values points
255 out that velocity data from the two missions can be well merged.

256 In addition to the recently generated velocity products we use velocity data from earlier years for
257 the scientific interpretation which were derived from SAR data of various satellite missions,
258 including ERS-1, ERS-2, Envisat ASAR, and ALOS PALSAR (Rott et al., 2002; 2011; 2014; Wuite
259 et al., 2015).

260 In order to obtain mass balance estimates by the input/output method, we compute the mass flux F
261 across a gate of width Y [m] at the calving front or grounding line according to:

$$F_Y = \rho_i \int_0^Y [u_m(y)H(y)] dy$$

262 ρ_i is the density of ice, u_m is the mean velocity of the vertical ice column perpendicular to the gate,
263 and H is the ice thickness. We use ice density of 900 kg m^{-3} to convert ice volume into mass. For
264 calving glaciers full sliding is assumed across calving fronts, so that u_m corresponds to the surface
265 velocity, u_s , obtained from satellite data. For glaciers discharging into the SCAR Inlet ice shelf we
266 estimated the ice deformation at the flux gates applying the laminar flow approximation (Paterson,
267 1994). The resulting vertically averaged velocity for these glaciers is $u_m = 0.95 u_s$. The ice thickness
268 at the flux gates is obtained from various sources. For some glaciers sounding data on ice thickness
269 are available, measured either by in situ or airborne radar sounders (Farinotti et al., 2013; 2014;
270 Leuschen et al. 2010, updated 2016). For glaciers with floating terminus the ice thickness is
271 deduced from the height above sea level applying the flotation criterion. For uncertainty estimates
272 of mass fluxes we assume $\pm 10 \%$ error for the cross section area of glaciers with GPR data across
273 or close to the gates and $\pm 15 \%$ for glaciers where the ice thickness is deduced from frontal height
274 above flotation. For velocities across the gates we assume $\pm 5 \%$ uncertainty. For the uncertainty of
275 surface mass balance at basin scale, based on RACMO output available at monthly time scale, we
276 assume $\pm 15 \%$ uncertainty.



277 **3. Elevation change and mass balance of glaciers north of Seal Nunataks**

278 **3.1 Elevation change and mass balance by DEM differencing**

279 The map of surface elevation change dh/dt from June/July 2013 to July/August 2016 for the glacier
280 basins discharging into PGC, Larsen Inlet and Larsen A embayment is shown in Figure 1. The
281 numbers on elevation change, volume change and mass balance, excluding floating glacier areas,
282 are specified in Table 1. As explained in Section 2.1, for areas not displayed in this map (steep radar
283 fore-slopes and the ice plateau above the escarpment) the available data indicate minimal changes in
284 surface elevation so that stable surface topography is assumed for estimating the net mass balance.

285 For glaciers with major sections of floating ice and frontal advance or retreat the extent, SEC and
286 volume change (including the subaqueous part) of the floating area and the advance/retreat area and
287 volume are specified in Table 2. The area extent of floating ice is inferred from the reduced rate of
288 SEC compared to grounded ice, using the height above sea level as additional constraint. Dinsmoor-
289 Bombardier-Edgeworth glaciers (DBE, basin A4) had the largest floating area (56.2 km^2) extending
290 about 8 km into a narrow fjord and showed also the largest frontal advance (11.7 km^2) between
291 2013 and 2016.

292 The mass depletion of grounded ice in the basins A1 to A7 (2.38 Gt a^{-1}) during the period 2013 to
293 2016 amounts to 60 % of the 2011 to 2013 depletion rate (3.98 Gt a^{-1} for the grounded areas; Rott et
294 al., 2014). The mass deficit is dominated by Drygalski Glacier (1.72 Gt a^{-1} for 2013 to 2016), down
295 from 2.18 Gt a^{-1} for 2011 to 2013. A decline of mass losses between the first and second period is
296 observed for all basins except A3 (Albone, Pyke, Polaris, Eliason glaciers, APPE) in Larsen Inlet
297 which was approximately in balanced state during 2011 to 2016.

298 The altitude dependence of elevation change (dh/dt) for the three basins with the largest mass
299 deficit is shown in Figure 2. Positive values in the lowest elevation zone of Basin A2 and A6 are
300 due to frontal advance. The areas close to the fronts include partly floating ice so that the observed
301 SEC is smaller than on grounded areas further upstream. The largest loss rates are observed in
302 elevation zones several km inland of the front.

303 **3.2 Flow velocities, calving fluxes and mass balance by the input/output method**

304 Data on flow velocities provide on one hand input for deriving calving fluxes, on the other hand
305 information for studying the dynamic response of the glaciers. Figure 3 shows maps of surface
306 velocities in 2011 and 2016, derived from TerraSAR-X and TanDEM-X 11-day repeat pass images,
307 and a map of the difference in velocity between November 1995 and 2016. The 1995 velocity map
308 was derived from interferometric one-day repeat pass data of crossing orbits from the satellites
309 ERS-1 and ERS-2 (map shown in Figure S3 of Rott et al., 2014, Supplementary Material). In



310 November 1995, ten months after ice shelf collapse, the velocities at calving fronts had already
311 accelerated significantly compared to pre-collapse conditions (Rott et al., 2002). Between 2011 and
312 2016 the flow velocities slowed down significantly. Even so, in 2016 the terminus velocities of the
313 major outlet glaciers still exceeded the November 1995 velocities.

314 Details on velocities along central flowlines of Drygalski, Edgeworth and Sjögren glaciers and the
315 position of calving fronts are shown in Figure 4 for different dates between 1995 and 2016. The
316 distance along the x-axis refers to the 1995 grounding line retrieved from ERS-1/ERS-2 InSAR data
317 (Rott et al., 2002). The front of the three glaciers retreated since 1995 by several kilometres, with
318 the largest retreat (11 km) by Sjögren Glacier in 2012. Between 2013 and 2016 the front of
319 Edgeworth Glacier advanced by 1.5 km and the front of Sjögren Glacier by 0.5 km.

320 Sjögren Glacier shows a gradual decrease of velocity from 2.9 m d^{-1} in August 2009 to 1.5 m d^{-1} in
321 October 2016, referring to the centre of the 2009 front. The velocity on Edgeworth Glacier
322 decreased from 2.5 m d^{-1} in October 2008 to 1.1 m d^{-1} in August 2016. The rate of deceleration
323 between 2013 and 2016 was particularly pronounced on the lowest 6 km of the terminus where the
324 ice was ungrounded. For Drygalski Glacier we show also pre-collapse velocities (January 1993),
325 derived from 35-day ERS-1 repeat pass images by offset tracking. In November 1995 the glacier
326 front was located near the pre-collapse grounding line, but the flow acceleration had already
327 propagated 10 km upstream of the front. Due to rapid flow the phase of the 31 October/1 November
328 1995 ERS-1/ERS-2 InSAR pair is decorrelated on the lowest two kilometres, prohibiting there
329 interferometric velocity retrieval. Velocities of January 1999 and November 2015 are similar, 7.0 m
330 d^{-1} at the location of the 2015 glacier front. Velocities were lower in 2007 to 2009, and higher in
331 2011 to 2014, reaching 8.8 m d^{-1} in November 2011.

332 The recent period of abating flow velocities coincides with years when the sea ice cover persisted
333 during summer. Time series of satellite SAR images show open water in front of the glaciers during
334 several summers up to summer 2008/09 and again in the summers 2010/2011 and 2011/2012. Sea
335 ice persisted all year round from winter 2012 onwards. Open leads in summer and the gradual drift
336 of ice that calved off from the glaciers indicate occasional moderate movement of sea ice.

337 Slowdown of calving velocities is the main cause for reduced mass deficits during the period 2013
338 to 2016 compared to previous years. Numbers on calving fluxes for 2011 to 2013 and 2013 to 2016
339 and the mass balance, derived by the IOM, are specified for four main glacier basins in Table 3. For
340 deriving the calving flux (CF) for each period a linear interpolation between the fluxes at the start
341 date and end date of the period is applied, including a correction for the time lag between ice
342 motion and topography data. If velocity data are available on additional dates in between, these are
343 also taken into account for temporal interpolation. Whereas the SMB between the periods 2011 to



344 2013 and 2013 to 2016 differs only by 2%, the combined annual calving flux of the four glaciers is
345 reduced by 16 % during 2013 to 2016 (Table 3). The decrease is even more pronounced when
346 calving fluxes on individual dates in 2011, 2013 and 2016 are compared. On Drygalski Glacier the
347 calving flux decreased from 4.03 Gt a⁻¹ in November 2011 to 3.34 Gt a⁻¹ in December 2013 and
348 2.92 Gt a⁻¹ in September 2016, a decrease by 28 % during the five years.

349 The differences in the mass balance by TDM SEC (Table 1) and IOM (Table3) are within the
350 specified uncertainty. For IOM the mass balance of the four glaciers sums up to $B_n = -3.26 \text{ Gt a}^{-1}$ for
351 2011 to 2013 and $B_n = -2.23 \text{ Gt a}^{-1}$ for 2013 to 2016. The corresponding numbers from SEC
352 analysis, after adding or subtracting the subaqueous mass changes, are $B_n = -3.01 \text{ Gt a}^{-1}$ and $B_n = -$
353 1.99 Gt a^{-1} for the two periods.

354 For Drygalski Glacier the mass balance numbers for the two periods are $B_n = -2.29 \text{ Gt a}^{-1}$ and $B_n = -$
355 1.80 Gt a^{-1} by IOM, and $B_n = -2.18 \text{ Gt a}^{-1}$ and $B_n = -1.80 \text{ Gt a}^{-1}$ (including the subaqueous part) by
356 TDM SEC analysis. The good agreement of the IOM and SEC mass balance values for Drygalski
357 Glacier backs up the RACMO estimate for SMB with specific net balance $b_n = 1383 \text{ kg m}^{-2}\text{a}^{-1}$. For
358 the period 1980 to 2016 the mean SMB for Drygalski Glacier by RACMO is 1.35 Gt a⁻¹. This is
359 more than twice the ice mass flux across the grounding line in pre-collapse state (0.58 Gt a⁻¹)
360 obtained as model output by Royston and Gudmundsson (2016) which would imply a highly
361 positive mass balance taking RACMO SMB as reference for mass input. Velocity measurements in
362 October/November 1994 at stakes on Larsen A Ice Shelf downstream of Drygalski Glacier show
363 values that are close to the average velocity of the 10-year period 1984 to 1994 (Rott et al., 1998;
364 Rack et al., 1999). This supports the assumption that the Larsen A tributary glaciers were
365 approximately in balanced state before ice shelf collapse.

366 **4. Elevation change and mass balance of Larsen B glaciers**

367 **4.1 Elevation change and mass balance by DEM differencing**

368 The map of surface elevation change dh/dt for the glacier basins discharging into the Larsen B
369 embayment and SCAR Inlet ice shelf is shown in Figure 5 for the period May/June 2011 to
370 June/July 2013 and in Figure 6 for June/July 2013 to July/August 2016. The numbers on elevation
371 change, volume change and mass balance, referring to grounded ice, are specified in Table 4 for
372 2011 to 2013 and in Table 5 for 2013 to 2016.

373 The SEC analysis shows large spatial and temporal differences in mass depletion between
374 individual glaciers. The overall mass deficit of the Larsen B region is dominated by glaciers
375 draining into the embayment where the ice shelf broke away in 2003 (basins B1 to B11). The annual
376 mass deficit of the glaciers draining into SCAR Inlet ice shelf (basins B12 to B17) remained modest



377 and was similar in both periods: $B_n = -0.54 \text{ Gt a}^{-1}$ during 2011 to 2013 and $B_n = -0.58 \text{ Gt a}^{-1}$ during
378 2013 to 2016. The small glaciers (B12 to B15) were in balanced state. The mass balance of Flask
379 and Leppard glaciers was slightly negative due to flow acceleration and increased ice export after
380 break-up of the main section of Larsen B Ice Shelf (Wuite et al., 2015).

381 In 2011 to 2013 the total annual net mass balance of basins B1 to B11 amounted to $B_n = -5.75 \text{ Gt a}^{-1}$
382 ¹, with the mass deficit dominated by Hektoria-Green (HG) glaciers ($B_n = -3.88 \text{ Gt a}^{-1}$), followed by
383 Crane Glacier ($B_n = -0.72 \text{ Gt a}^{-1}$). The mass losses of Evans and Jorum glaciers and of basin B1
384 (northeast of Hektoria Glacier) were also substantial, whereas the mass deficit of the other glaciers
385 was modest. During the period 2013 to 2016 the annual mass deficit of the glacier ensemble was cut
386 by more than half ($B_n = -2.32 \text{ Gt a}^{-1}$) compared to 2011 to 2013, with again HG dominating the
387 mass loss ($B_n = -1.54 \text{ Gt a}^{-1}$). The decrease in mass depletion was also significant for other glaciers.
388 For Crane Glacier the 2013 to 2016 loss rate ($B_n = -0.22 \text{ Gt a}^{-1}$) corresponds to only 18 % of the
389 estimated balance flux (Rott et al., 2011), a large drop since 2007 with $B_n = -3.87 \text{ Gt a}^{-1}$ (Wuite et
390 al., 2015).

391 The decline of mass depletion coincided with a period of permanent sea ice cover starting in
392 autumn/winter 2011. During several summers before, including summer 2010/11, the sea ice in
393 front of the glaciers drifted away and gave way to extended periods with open water. During the
394 years thereafter the continuous sea ice over obstructed the detachment of frontal ice and facilitated
395 frontal advance. The maximum terminus advance was observed for HG glaciers, resulting in an
396 increase of glacier area of 31.6 km^2 from 2011 to 2013 and 48.0 km^2 from 2013 to 2016 (Table 6).

397 Due to significant decrease in ice thickness the floating area on Hektoria and Green glaciers
398 increased significantly after 2011, covering in June 2013 an area of 19.8 km^2 and in June 2016 an
399 area of 62.1 km^2 in addition to the frontal advance areas 2011 to 2013, respectively 2013 to 2016,
400 where the ice was almost completely ungrounded. Areas of floating ice, covering some km^2 in area,
401 were observed on Evans Glacier and Crane Glacier, increasing significantly between 2013 and
402 2016. The areas of frontal advance showed a similar temporal trend, with an increase of 3.7 km^2
403 between 2011 and 2013 and 5.4 km^2 between 2013 and 2016 for Evans Glacier, and 5.0 km^2 and
404 10.5 km^2 for Crane Glacier.

405 Figure 7 shows the altitude dependence of elevation change (dh/dt) for four basins with large mass
406 deficits. The largest drawdown rate (19.5 m a^{-1}) was observed on HG glaciers in the elevation zone
407 200 m to 300 m a.s.l. during 2011 to 2013, with substantial drawdown up to the 1000 m elevation
408 zone. On Jorum Glacier the area affected by surface lowering extended up to 700 m elevation, with
409 a maximum rate of 5 m a^{-1} . The drawdown pattern of Crane Glacier is different, with the zone of the
410 largest 2011 to 2013 drawdown rates (4.5 m a^{-1}) commencing about 30 km inland of the front,



411 extending across the elevation range 500 m to 850 m, abating and shifting further upstream in 2013
412 to 2016. Scambos et al. (2011) observed an anomalous drawdown pattern on the Crane terminus
413 during the first few years after ice shelf collapse, very likely associated with drainage of a
414 subglacial lake.

415 **4.2 Flow velocities, calving fluxes and mass balance by the input/output method**

416 Figure 8 shows maps of surface velocities in 2011 and 2016 and a map of the differences in velocity
417 between November 1995 and 2016. Gaps in the 2011 TerraSAR-X/TanDEM-X velocity map are
418 filled up with PALSAR data and in the 2016 map with Sentinel-1 data. The 1995 velocity map used
419 as reference for pre-collapse conditions, was derived from ERS one-day interferometric repeat pass
420 data. The ERS data show very little difference between 1995 and 1999 flow velocities, suggesting
421 that the glaciers were close to balanced state during those years (Rott et al, 2011). In 2016 the
422 velocities of the main glaciers were still higher than in 1995, but had slowed down significantly
423 since 2011.

424 The temporal evolution of Larsen B glaciers between 1995 and 2013 is described in detail by Wuite
425 et al. (2015), showing velocity maps for 1995 and 2008-2012 and time series of velocities along
426 central flowlines of eight glaciers between 1995 and 2013. In extension, we report here velocity
427 changes since 2013 and provide details on velocities of HG and Crane glaciers in recent years,
428 including a diagram of velocities across the flux gates on different dates (Figure 9).

429 The glaciers discharging into SCAR Inlet ice shelf and the small glaciers of the main Larsen B
430 embayment (B4, B5, B8 to B11) showed only small variations in velocity since 2011, though in
431 2016 the velocities of these glaciers were still higher than during the pre-collapse period. The main
432 glaciers were subject to significant slowdown. On Crane Glacier the velocity in the centre of the
433 flux gate decreased from a value of 6.8 m d^{-1} in July 2007 to 3.9 m d^{-1} in September 2011, 2.9 m d^{-1}
434 in November 2013 and 2.4 m d^{-1} in October 2016, still 50 % higher than the velocities in 1995 and
435 1999. Because of major glacier thinning, the cross section of the flux gate decreased significantly,
436 so that the calving flux amounted in mid-2016 to 1.39 Gt a^{-1} , only 20 % larger than in 1995 to 1999.
437 Since 2007 the drawdown rate of Crane Glacier decreased steadily, from a mass balance $B_n = -3.87$
438 Gt a^{-1} in June 2007 to $B_n = -0.23 \text{ Gt a}^{-1}$ in November 2016. Also on Jorum Glacier the calving
439 velocity decreased gradually since 2007; during 2013 to 2016 the glacier was close to balanced
440 state. On the other hand the velocity at the flux gate of Melville Glacier was in 2011 to 2016 only
441 5 % lower than in 2008, 2.6 times higher than the pre-collapse velocity reported by Rott et al.
442 (2011). This agrees with the negative mass balance by TDM SEC analysis. However, the mass
443 deficit is small in absolute terms because of the modest mass turnover.



444 The velocities of Hektoría and Green glaciers have been subject to significant variations since 2002,
445 associated with major frontal retreat but also intermittent periods of frontal advance (Wuite et al.,
446 2015). Between November 2008 and November 2009 the velocity in the centre of the Hektoría flux
447 gate increased from 1.4 m d^{-1} to 2.8 m d^{-1} , slowed down slightly during 2010, and accelerated again
448 in 2011 to reach a value of 4.2 m d^{-1} in November 2011, followed by deceleration to 3.5 m d^{-1} in
449 March 2012, 2.0 m d^{-1} in July 2013 and 1.4 m d^{-1} in June 2016 (Figure 9). Similar deceleration was
450 observed for Green Glacier, from 4.6 m d^{-1} in November 2011, to 2.8 m d^{-1} in July 2013 and 2.0 m
451 d^{-1} in June 2016.

452 The slowdown and frontal advance of Larsen B calving glaciers coincided with a period of
453 continuous sea ice cover since mid-2011, indicating significant impact of pre-frontal marine
454 conditions on ice flow. Tracking of detached ice blocks close to glacier fronts shows for 2013 to
455 2016 the following displacements: 6.1 km for Crane Glacier, 2.7 km for Melville Glacier, 2.5 km
456 for Jorum Glacier and 0.9 km for Mapple Glacier. This corresponds to about twice the flux gate
457 velocity for Crane Glacier and about five times for Melville Glacier. The 2013 to 2016 displacement
458 of ice blocks in front of HG glaciers (4.5 km for Green, 3.9 km for Hektoría) exceeded only slightly
459 the distance of frontal advance.

460 The comparison of mass balance by IOM (Table 7) and SEC shows good overall agreement, as well
461 as for most of the individual basins. The combined 2011 to 2013 annual mass balance of the five
462 basins discharging into the main Larsen B embayment (B2, B3, B6, B7, B10) is $B_n = -5.26 \text{ Gt a}^{-1}$ by
463 TDM SEC and $B_n = -5.63 \text{ Gt a}^{-1}$ by IOM, and for 2013 to 2016 $B_n = -2.15 \text{ Gt a}^{-1}$ by TDM SEC and
464 $B_n = -2.28 \text{ Gt a}^{-1}$ by IOM. The SEC mass balance in this comparison includes also the volume
465 change of the floating glacier sections (Table 6). Also for Starbuck and Flask glaciers (B13, B16)
466 the mass balance values of the two methods agree well. The only basin where the difference
467 between the two methods exceeds the estimated uncertainty is Leppard Glacier (B17), where IOM
468 ($B_n = -0.89 \text{ Gt a}^{-1}$ and $B_n -0.82 \text{ Gt a}^{-1}$ for the two periods) shows larger losses than SEC ($B_n = -0.21$
469 Gt a^{-1} and $B_n -0.30 \text{ Gt a}^{-1}$). The SEC retrievals of the basins B3, B7, B10, B13, B16, which show
470 good agreement between SEC and IOM mass balance, are based on data of the same TDM track as
471 B17. Therefore it can be concluded that the difference in MB of Leppard Glacier is probably due to
472 a bias either in SMB or in the cross section of the flux gate, or in both. The specific surface mass
473 balance (Table 7) for the adjoining Flask Glacier is 39 % higher than for Leppard Glacier.

474 5. Discussion

475 The main outlet glaciers to the northern sections of Larsen Ice Shelf that disintegrated in 1995
476 (Prince-Gustav-Channel and Larsen A ice shelves, PGC-LA) and in 2002 (the main section of
477 Larsen B Ice Shelf) are still losing mass due to dynamic thinning. The losses are caused by



478 accelerated ice flow tracing back to the reduction of backstress after ice shelf break-up triggering
479 dynamic instabilities (Rott et al., 2002; 2011; Scambos et al., 2004; Wuite et al., 2015; De Rydt
480 et al., 2015; Royston and Gudmundsson, 2016).

481 On the outlet glaciers to PGC-LA (basins A1 to A7) the rate of mass depletion of grounded ice
482 decreased by 40 % from $3.98 \pm 0.33 \text{ Gt a}^{-1}$ during the period 2011 to 2013 to $2.38 \pm 0.18 \text{ Gt a}^{-1}$
483 during 2013 to 2016. The mass deficit of the area was dominated by losses of Drygalski Glacier,
484 with annual mass balance $B_n = -2.18 \text{ Gt a}^{-1}$ in 2011 to 2013 and $B_n = -1.72 \text{ Gt a}^{-1}$ in 2013 to 2016.
485 Scambos et al. (2014) report for 2001 to 2008 a mass change of -5.67 Gt a^{-1} for glacier basins 21 to
486 25, corresponding approximately to our basins A1 to A7. On Drygalski Glacier the 2003 to 2008
487 rate of mass depletion ($B_n = -2.39 \text{ Gt a}^{-1}$) by Scambos et al. (2014) was only 9 % higher than our
488 estimate for 2011 to 2013. On the other glaciers of PGC and Larsen A embayment the slow-down
489 of calving velocities and decrease in calving fluxes during the last decade was more pronounced.

490 On the outlet glaciers to Larsen B embayment (basins B1 to B11) the rate of mass depletion for
491 grounded ice decreased by 60 % from $5.75 \pm 0.45 \text{ Gt a}^{-1}$ during 2011 to 2013 to $2.32 \pm 0.25 \text{ Gt a}^{-1}$
492 during 2013 to 2016. Hektoria and Green glaciers accounted in both periods for the bulk of the mass
493 deficit ($B_n = -3.88 \text{ Gt a}^{-1}$, $B_n = -1.54 \text{ Gt a}^{-1}$). High drawdown rates were observed on HG glaciers
494 during 2011 to 2013, with the maximum value (19.5 m a^{-1}) in the elevation zone 200 m to 300 m
495 a.s.l. Our basins B1 to B11 correspond to the basins 26a and 27 to 31a of Scambos et al. (2014).
496 Based on ICESat data spanning September 2003 to March 2008 and optical stereo image DEMs
497 acquired between November 2001 to November 2006, Scambos et al. (2014) report for these basins
498 an annual mass balance $B_n = -8.39 \text{ Gt a}^{-1}$ excluding ice lost by frontal retreat. Our rate of mass loss
499 for 2011 to 2013 amounts to 69% of this value, and for 2013 to 2016 to 36%, a similar percentage
500 decrease of mass losses as for the PGC-LA basins. After ice shelf break-up in March 2002 glacier
501 flow accelerated rapidly, causing large increase of calving fluxes during the first years after Larsen
502 B collapse, whereas on most glaciers the calving velocities slowed down significantly after 2007
503 (Scambos et al., 2004, 2011; Rott et al., 2011; Shuman et al., 2011; Wuite et al., 2015). An
504 exception is basin B2 (HG glaciers) for which the 2011 to 2013 loss rate was 2% higher than the
505 value ($B_n = -3.82 \text{ Gt a}^{-1}$) reported by Scambos et al. (2014) for 2001 to 2008.

506 The drawdown pattern on the main glaciers shows high elevation loss rates for grounded ice shortly
507 upstream of the glacier front or upstream of the floating glacier section, and abating loss rates
508 towards higher elevation. This is the typical loss pattern for changes in the stress state at the
509 downstream end of a glacier as response to the loss of terminal floating ice (Hulbe et al., 2008). The
510 elevation change pattern of recent years is different on Crane Glacier, where elevation decline and
511 thinning migrated up-glacier during 2011 to 2016, an indication for upstream-propagating



512 disturbances (Pfeffer, 2007). Both patterns indicate that the glaciers are still away from equilibrium
513 state and dynamic thinning will continue for years.

514 We compiled surface motion and calving fluxes for main glaciers of the study region and derived
515 the surface mass balance from output of the regional atmospheric climate model RACMO. These
516 data enable to compare individual components of the mass balance. Whereas the SMB differed
517 between the periods 2011 to 2013 and 2013 to 2016 only by few per cent, the calving fluxes
518 decreased significantly due to slow-down of ice motion, confirming that the mass losses were of
519 dynamic origin, an aftermath to changes in the stress regime after ice shelf collapse.

520 The terminus velocities on most glaciers are still higher than during the pre-collapse period. After
521 rapid flow acceleration during the first years after ice shelf break-up there has been a general trend
522 of deceleration afterwards, however with distinct differences in the temporal pattern between
523 individual glaciers. Glaciers with broad calving fronts show larger temporal variability of velocities
524 and calving fluxes than glaciers with small width to length ratio. In the Larsen A embayment the
525 Drygalski Glacier has been subject to major variations in flow velocity and calving flux during the
526 last decade. In 2007 to 2009 the velocity in the centre of the flux gate varied between 5.5 m d^{-1} and
527 6 m d^{-1} , increased to 8 m d^{-1} in 2011 and 2012, and decreased to 6.0 m d^{-1} in July 2016, still four
528 times higher than the velocity in 1993. In the Larsen B embayment Hektor and Green glaciers
529 showed large temporal fluctuation in velocity and a general trend of frontal retreat, but also sporadic
530 periods of frontal advance. A major intermittent acceleration event, starting in 2010, was
531 responsible for a large mass deficit in 2011 to 2013.

532 Regarding the SCAR Inlet ice shelf tributaries, the small glaciers (basin B12 to B15) were
533 approximately in balanced state, whereas Flask (B16) and Leppard (B17) glaciers had a moderate
534 mass deficit. The total mass balance of the SCAR Inlet glaciers, based on TDM SEC analysis, was
535 $B_n = -0.54 \pm 0.38 \text{ Gt a}^{-1}$ in 2011 to 2013 and $B_n = -0.58 \pm 0.38 \text{ Gt a}^{-1}$ in 2013 to 2016. As for the
536 calving glaciers to the Larsen A and B embayments, the loss rate was lower than during the period
537 2001 to 2008 ($B_n = -1.37 \text{ Gt a}^{-1}$) reported by Scambos et al. (2014).

538 The slowdown of flow velocities and decline in mass depletion between 2011 and 2016 coincided
539 with periods of continuous sea ice cover. After several summers with open water (excluding
540 summer 2009/10 when sea ice persisted), a period of permanent sea ice cover in front of the glaciers
541 commenced in Larsen B embayment in winter 2011 and in PGC and Larsen A embayment in winter
542 2013. The sea ice cover impeded glacier calving, as apparent in frontal advance of several glaciers.
543 Large frontal advance was observed for HG glaciers ($\sim 3.2 \text{ km}$ during 2011 to 2013 and $\sim 3.8 \text{ km}$
544 during 2013 to 2016) and Crane Glacier ($\sim 1.2 \text{ km}$ during 2011 to 2013 and $\sim 2.5 \text{ km}$ during 2013 to



545 2016). The front of Bombardier-Edgeworth glaciers advanced between 2013 and 2016 by 1.5 km
546 and the front of Sjøgren Glacier by 0.5 km. The continuous sea ice cover and restricted movement
547 of ice calving off from glaciers contrasts with the rapid movement of icebergs during the first few
548 days after Larsen A and B collapse, drifting away by up to 20 km per day due to strong downslope
549 winds and local ocean currents (Rott et al., 1996; Rack and Rott 2004). For 2006 to 2015 a modest
550 trend of atmospheric cooling was observed in the study region, in particular in summer (Turner et
551 al., 2016; Oliva et al., 2017). However, this feature does not fully explain the striking difference in
552 sea ice pattern and ice drift.

553 6. Conclusions

554 The analysis of surface elevation change by DEM differencing over the periods 2011 to 2013 and
555 2013 to 2016 shows continuing drawdown and major losses in ice mass for outlet glaciers to Prince-
556 Gustav-Channel and the Larsen A and B embayments. During the observation period 2011 to 2016
557 there was a general trend of decreasing mass depletion, induced by slowdown of calving velocities
558 resulting in reduced calving fluxes. For several glaciers frontal advance was observed in spite of
559 ongoing elevation losses upstream. The mass balance numbers for the glaciers north of Seal
560 Nunataks are $B_n = -3.98 \pm 0.33 \text{ Gt a}^{-1}$ during 2011 to 2013 and $B_n = -2.38 \pm 0.18 \text{ Gt a}^{-1}$ during 2013
561 to 2016. The corresponding numbers for glaciers calving into the Larsen B embayment for the two
562 periods are $B_n = -5.75 \pm 0.45 \text{ Gt a}^{-1}$ and $B_n = -2.32 \pm 0.25 \text{ Gt a}^{-1}$. For the glacier discharging into
563 SCAR Inlet ice shelf the losses were modest.

564 The period of decreasing flow velocities and frontal advance coincides with several years when the
565 sea ice cover persisted during summer. Considering the ongoing mass depletion and the increase of
566 ungrounded glacier area due to thinning, we expect recurrence of periods with frontal retreat and
567 increasing calving fluxes, in particular for those glaciers that showed major temporal variations in
568 ice flow during the last several years.

569 In Larsen A embayment large fluctuations in velocity were observed for Drygalski Glacier, and in
570 Larsen B embayment for Hektoría and Green glaciers. These are the glaciers with the main share in
571 the overall mass losses of the region: Drygalski Glacier contributed 61 % to the 2011 to 2016 mass
572 deficit of the Larsen A/PGC outlet glaciers, and HG glaciers accounted for 67 % of the mass deficit
573 of the Larsen B glaciers. On HG glaciers the ice flow accelerated significantly in 2010/2011,
574 triggering elevation losses up to 19.5 m a^{-1} on the lower terminus during the period 2011 to 2013.
575 HG glaciers have a joint broad calving front and the frontal sections are ungrounded, thus being
576 more vulnerable to changes in atmospheric and oceanic boundary conditions than glaciers that are
577 confined in narrow valleys.



578 Complementary to DEM differencing, we applied the input/output method to derive the mass
579 balance of the main glaciers. The mass balance numbers of these two independent methods show
580 good agreement, affirming the soundness of the reported results. The agreement backs up also the
581 reliability of the RACMO SMB data. A strong indicator for the good quality of the TDM SEC
582 products is the good agreement with 2011-2016 SEC data measured by the airborne laser scanner of
583 NASA IceBridge. Both data sets were independently processed. The agreement indicates that SAR
584 signal penetration does not affect the retrieval of surface elevation change on glaciers by InSAR
585 DEM differencing if repeat observation data are acquired over snow/ice media with stable
586 backscatter properties under the same observation geometry.

587

588 *Data availability.* Data sets used in this study will be made available upon publication of the final
589 version on cryoportal.enveo.at.

590 *Competing interests.* The authors declare that they have no conflict of interest.

591

592 *Acknowledgements.* The TerraSAR-X data and TanDEM-X data were made available by DLR
593 through projects HYD1864, XTI_GLAC1864, XTI_GLAC6809 and DEM_GLA1059. Sentinel- 1
594 data were obtained through the ESA Sentinel Scientific Data Hub, ALOS PALSAR data through the
595 ESA ALDEN AOALO 3741 project. Landsat 8 images, available at USGS Earth Explorer, were
596 downloaded via Libra browser. The IceBridge ATM L4 Surface Elevation Rate of Change and
597 IceBridge MCoRDS Ice Thickness version V001 data were downloaded from the NASA
598 Distributed Active Archive Center, US National Snow and Ice Data Center (NSIDC), Boulder,
599 Colorado. We wish to thank A. Cook (Univ. Swansea, UK) for providing outlines of glacier basins.
600 The work was supported by the European Space Agency, ESA Contract No. 4000115896/15/I-LG,
601 High Resolution SAR Algorithms for Mass Balance and Dynamics of Calving Glaciers (SAMBA).

602

603 **References**

604 Abdel Jaber, W.: Derivation of mass balance and surface velocity of glaciers by means of high
605 resolution synthetic aperture radar: application to the Patagonian Icefields and Antarctica, Doctoral
606 Thesis, Technical University of Munich, DLR Research Report 2016-54, 236 pp, 2016.

607 Berthier, E., Scambos, T. A., and Shuman, C. A.: Mass loss of Larsen B tributary glaciers (Antarctic
608 Peninsula) unabated since 2002, *Geophys. Res. Lett.*, 39, L13501, doi:10.1029/2012GL051755, 2012.



- 610 Cook, A. J., Murray, T., Luckman, A., Vaughan, D. G., and Barrand, N. E.: A new 100-m digital
611 elevation model of the Antarctic Peninsula derived from ASTER Global DEM: Methods and
612 accuracy assessment, *Earth Syst. Sci. Data*, 4, 129–142, doi:10.5194/essd-4-129-2012, 2012.
- 613 Cook, A. J., Vaughan, D. G., Luckman, A., and Murray, T.: A new Antarctic Peninsula glacier basin
614 inventory and observed area changes since the 1940s, *Antarctic Science*, 26(6), 614-624, 2014.
- 615 De Rydt, J., Gudmundsson, G. H., Rott, H., and Bamber, J. L.: Modelling the instantaneous
616 response of glaciers after the collapse of the Larsen B Ice Shelf, *Geophys. Res. Lett.*, 42(13), 5355–
617 5363, doi: 10.1002/2015GL064355, 2015.
- 618 De Angelis, H. and Skvarca, P.: Glacier surge after ice shelf collapse, *Science*, 299 (5612), 1560–
619 1562, doi:10.1126/science.1077987, 2003.
- 620 Farinotti, D., Corr, H. F. J., and Gudmundsson, G. H.: The ice thickness distribution of Flask
621 Glacier, Antarctic Peninsula, determined by combining radio-echo soundings, surface velocity data
622 and flow modelling, *Ann. Glaciol.*, 54 (63), doi:10.3189/2013AoG63A603, 2013.
- 623 Farinotti, D., King, E. C., Albrecht, A., Huss, M., and Gudmundsson, G. H.: The bedrock
624 topography of Starbuck Glacier, Antarctic Peninsula, as measured by ground based radio-echo
625 soundings, *Ann. Glaciol.*, 55, 22–28, 2014.
- 626 Glasser, N. F. and Scambos, T. A.: A structural glaciological analysis of the 2002 Larsen B ice-shelf
627 collapse, *J. Glaciol.*, 54, 3–16, 2008.
- 628 Hulbe, C. L., Scambos, T. A., Youngberg, T., and Lamb, A.K.: Patterns of glacier response to
629 disintegration of the Larsen B ice shelf, Antarctic Peninsula, *Global Planet. Change*, 63(1), 1–8,
630 2008.
- 631 Khazendar, A., Borstad, C. P., Scheuchl, B., Rignot, E., and Seroussi, H.: The evolving instability of
632 the remnant Larsen B Ice Shelf and its tributary glaciers, *Earth and Planetary Science Letters*,
633 419(199), 2015.
- 634 Krieger, G., Zink, M., Bachmann, M., Bräutigam, B., Schulze, D., Martone, M., Rizzoli, P.,
635 Steinbrecher, U., Anthony, J. W., De Zan, F., Hajnsek, I., Papathanassiou, K., Kugler, F., Rodriguez
636 Cassola, M., Younis, M., Baumgartner, S., Lopez Dekker, P., Prats, P., and Moreira, A.: TanDEM-X:
637 a radar interferometer with two formation flying satellites, *Acta Astronaut.*, 89, 83–98,
638 doi:10.1016/j.actaastro.2013.03.008, 2013.
- 639 Lachaise, M. and Fritz, T.: Phase unwrapping strategy and assessment for the high resolution DEMs
640 of the TanDEM-X mission, in: *Proc. of IEEE Geoscience and Remote Sensing Symposium*
641 (IGARSS), 10-15 July 2016, Beijing, China, pp. 3223-3226, 2016.



- 642 Leuschen, C., Gogineni, P., Rodriguez-Morales, F., Paden, J., and Allen, C.: IceBridge MCoRDS L2
643 Ice Thickness, Boulder, Colorado USA. NASA National Snow and Ice Data Center Distributed
644 Active Archive Center, doi: <http://dx.doi.org/10.5067/GDQ0CUCVTE2Q>, 2010, updated 2016.
- 645 Nagler, T., Rott, H., Hetzenecker, M., Wuite, J., and Potin, P.: The Sentinel-1 Mission: New
646 opportunities for ice sheet observations, *Remote Sensing*, 7(7), 9371-9389;
647 doi:10.3390/rs70709371, 2015.
- 648 Oliva, M., Navarro, F., Hrbáček, F., Hernández, A., Nývlt, D., Pereira, P., Ruiz-Fernández, J., and
649 Trigo, R.: Recent regional climate cooling on the Antarctic Peninsula and associated impacts on the
650 cryosphere, *Sci. Total Environ.*, 580, 210–223, doi:10.1016/j.scitotenv.2016.12.030, 2017.
- 651 Paterson, W. S. B.: *The physics of glaciers*, Third Edition, Oxford, etc., Elsevier, 1994.
- 652 Pfeffer, W. T.: A simple mechanism for irreversible tidewater glacier retreat, *J. Geophys. Res.-Earth*,
653 112, F03S25, doi:10.1029/2006JF000590, 2007.
- 654 Rack, W. and Rott, H.: Pattern of retreat and disintegration of Larsen B Ice Shelf, Antarctic
655 Peninsula, *Ann. Glaciol.*, 39, 505-510, 2004.
- 656 Rack W., Rott, H., Skvarca, P., and Siegel, A.: The motion field of northern Larsen Ice Shelf derived
657 from satellite imagery, *Ann. Glaciol.*, 29, 261-266, 1999.
- 658 Rignot, E., Casassa, G., Gogineni, P., Rivera, A., and Thomas, R.: Accelerated ice discharges from
659 the Antarctic Peninsula following the collapse of the Larsen B Ice Shelf, *Geophys. Res. Lett.*, 31,
660 L18401, doi:10.1029/2004GL020697, 2004.
- 661 Rizzoli, P., Bräutigam, B., Kraus, T., Martone, M., and Krieger, G.: Relative height error analysis of
662 TanDEM-X elevation data, *ISPRS J. Photogrammet. Remote Sens.*, 73, 30–38, 2012.
- 663 Rizzoli, P., Martone, M., Rott, H., and Moreira, A.: Characterization of snow facies on the
664 Greenland Ice Sheet observed by TanDEM-X interferometric SAR data, *Remote Sens.*, 9 (4), 315;
665 doi:10.3390/rs9040315, 2017.
- 666 Rossi, C., Rodriguez Gonzalez, F., Fritz, T., Yague-Martinez, N., and Eineder, M.: TanDEM-X
667 calibrated Raw DEM generation, *ISPRS J. Photogrammet. Remote Sens.*, 73, 12 - 20, doi:
668 10.1016/j.isprsjprs.2012.05.014, 2012.
- 669 Rott, H.: Advances in interferometric synthetic aperture radar (InSAR) in earth system science,
670 *Progress in Phys. Geogr.*, 33(6), 769-791, doi: 10.1177/0309133309350263, 2009.
- 671 Rott, H., Skvarca, P., and Nagler, T.: Rapid collapse of Northern Larsen Ice Shelf, Antarctica,
672 *Science*, 271, 788–792, 1996.



- 673 Rott H., Rack, W., Nagler, T., and Skvarca, P.: Climatically induced retreat and collapse of Northern
674 Larsen Ice Shelf, Antarctic Peninsula, *Ann. Glaciol.*, 27, 86-92, 1998.
- 675 Rott, H., Rack, W., Skvarca, P., and De Angelis, H.: Northern Larsen Ice Shelf, Antarctica: Further
676 retreat after collapse, *Ann. Glaciol.*, 34, 277– 282, 2002.
- 677 Rott, H., Müller, F., Nagler, T., and Floricioiu, D.: The imbalance of glaciers after disintegration of
678 Larsen B Ice Shelf, Antarctic Peninsula, *The Cryosphere*, 5 (1), 125–134, doi:10.5194/tc-5-125-
679 2011, 2011.
- 680 Rott, H., Floricioiu, D., Wuite, J., Scheiblauer, S., Nagler, T., and Kern, M.: Mass changes of outlet
681 glaciers along the Nordensjøkøld Coast, northern Antarctic Peninsula, based on TanDEM-X satellite
682 measurements, *Geophys. Res. Lett.*, 41, doi:10.1002/2014GL061613, 2014.
- 683 Royston, S., and Gudmundsson, G. H.: Changes in ice-shelf buttressing following the collapse of
684 Larsen A Ice Shelf, Antarctica, and the resulting impact on tributaries, *J. Glaciol.*, 62(235) 905–911,
685 2016.
- 686 Scambos, T. A., Bohlander, J. A., Shuman, C. A., and Skvarca, P.: Glacier acceleration and thinning
687 after ice shelf collapse in the Larsen B embayment, Antarctica, *Geophys. Res. Lett.*, 31, L18402,
688 doi:10.1029/2004GL020670, 2004.
- 689 Scambos, T. A., Berthier, E., and Shuman, C. A.: The triggering of subglacial lake drainage during
690 rapid glacier drawdown: Crane Glacier, Antarctic Peninsula, *Ann. Glaciol.*, 52(59), 74-82, 2011.
- 691 Scambos, T. A., Berthier, E., Haran, T., Shuman, C. A., Cook, A. J., Ligtenberg, S. R. M., and
692 Bohlander, J.: Detailed ice loss pattern in the northern Antarctic Peninsula: widespread decline
693 driven by ice front retreats, *The Cryosphere*, 8, 2135-2145, doi:10.5194/tc-8-2135-2014, 2014.
- 694 Schwerdt, M., Bräutigam, B., Bachmann, M., Döring, B., Schrank, D., Gonzalez, J. H.: Final
695 TerraSAR-X calibration results based on novel efficient methods, *IEEE Trans. Geosc. Rem. Sens.*,
696 48 (2), 677–689, 2010.
- 697 Seehaus, T., Marinsek, S., Helm, V., Skvarca, P., and Braun, M.: Changes in ice dynamics, elevation
698 and mass discharge of Dinsmoor–Bombardier–Edgeworth glacier system, Antarctic Peninsula,
699 *Earth Planet. Sci. Lett.* 427, 125–135. doi: 10.1016/j.epsl.2015.06.047, 2015.
- 700 Seehaus, T. C., Marinsek, S., Skvarca, P., van Wessem, J. M., Reijmer, C. H., Seco, J. L., and Braun,
701 M. H.: Dynamic response of Sjögren Inlet glaciers to ice shelf breakup - a remote sensing data
702 analysis, *Front. Earth Sci.* 4:66, doi: 10.3389/feart.2016.00066, 2016.
- 703 Shuman, C. A., Berthier, E., and Scambos, T. A.: 2001–2009 elevation and mass losses in the
704 Larsen A and B embayments, Antarctic Peninsula, *J. Glaciol.*, 57, 737–754, 2011.



- 705 Studinger, M. S: IceBridge ATM L4 Surface Elevation Rate of Change, Version 1, Subset M699,
706 S10, NASA Distributed Active Archive Center, National Snow and Ice Data Center, Boulder,
707 Colorado USA, 2014, updated 2017, doi: <http://dx.doi.org/10.5067/BCW6CI3TXOCY>, [Accessed
708 25 July 2017].
- 709 Torres, R., Snoeij, P., Geudtner, D., Bibby, D., Davidson, M., Attema, E., Potin, P., Rommen, B.,
710 Flourey, N., Brown, M., Navas Travera, I., Deghaye, P., Duesmann, B., Rosich, B., Miranda, N.,
711 Bruno, C., L'Abbate, M., Croci, R., Pietropaolo, A., Huchler, M., Rostan, F.: GMES Sentinel-1
712 mission, *Remote Sens. Environ.*, 120, 9–24, 2012.
- 713 Turner, J., Lu, H., White, I., King, J. C., Phillips, T., Hosking, J. S., Bracegirdle, T. J., Marshall, G.
714 J., Mulvaney, R. and Deb, P.: Absence of 21st century warming on Antarctic Peninsula consistent
715 with natural variability, *Nature*, 535, 411–415, doi:10.1038/nature18645, 2016.
- 716 van Wessem, J. M., Ligtenberg, S. R. M., Reijmer, C. H., van de Berg, W. J., van den Broeke, M.
717 R., Barrand, N. E., Thomas, E. R., Turner, J., Wuite, J., Scambos, T. A., and van Meijgaard, E.: The
718 modelled surface mass balance of the Antarctic Peninsula at 5.5 km horizontal resolution, *The
719 Cryosphere*, 10, 271-285, 2016.
- 720 van Wessem, J. M., van de Berg, W. J., Noël, B. P. Y., van Meijgaard, E., Birnbaum, G., Jakobs, C.
721 L., Krüger, K., Lenaerts, J. T. M., Lhermitte, S., Ligtenberg, S. R. M., Medley, B., Reijmer, C. H.,
722 van Tricht, K., Trusel, L. D., van Ulf, L. H., Wouters, B., Wuite, J., and van den Broeke, M. R.:
723 Modelling the climate and surface mass balance of polar ice sheets using RACMO2, part 2:
724 Antarctica (1979–2016), *The Cryosphere Discuss.*, <https://doi.org/10.5194/tc-2017-202>, in review,
725 2017.
- 726 Walter Antony, J. M., Schmidt, K., Schwerdt, M., Polimeni, D., Tous Ramon, N., Bachmann M.,
727 and Gabriel Castellanos, A.: Radiometric accuracy and stability of TerraSAR-X and TanDEM-X,
728 *Proceedings of the European Conference on Synthetic Aperture Radar (EUSAR)*, 6 – 9 June 2016,
729 Hamburg, Germany.
- 730 Wuite, J., Rott, H., Hetzenecker, M., Floricioiu, D., De Rydt, J., Gudmundsson, G. H., Nagler, T.,
731 and Kern, M.: Evolution of surface velocities and ice discharge of Larsen B outlet glaciers from
732 1995 to 2013, *The Cryosphere*, 9, 957-969, doi:10.5194/tc-9-957-2015, 2015.

733

734 **Tables**

735 **Table 1.** Rates of surface elevation change, volume change and mass balance by means of TDM
 736 DEM differencing 2013 to 2016, for glacier basins discharging into Prince-Gustav-Channel, Larsen
 737 Inlet and Larsen A embayment. dh/dt is the mean rate of elevation change of the area covered by
 738 the high resolution map (Fig. 1). The basin area refers to ice front positions delineated in TanDEM-
 739 X images of 2016-07-16, 2016-07-27, 2016-08-18. The rates of ice volume change (dV/dt) and total
 740 mass balance (dM/dt) refer to grounded ice. * dM/dt 2011-2013 for grounded areas of basins A1 to
 741 A7 from the TDM SEC analysis by Rott et al., (2014).

ID	Basin name	Basin area [km ²]	dh/dt map [km ²]	dh/dt [m a ⁻¹]	dV/dt [km ³ a ⁻¹]	Uncertainty [km ³ a ⁻¹]	dM/dt [Gt a ⁻¹] 2013-16	* dM/dt [Gt a ⁻¹] 2011-13
A1	Cape Longing Peninsula	668.9	576.9	-0.257	-0.146	±0.041	-0.131	-0.150
A2	Sjögren-Boydell (SB)	527.6	188.0	-1.239	-0.241	±0.046	-0.217	-0.364
A3	APPE glaciers	513.6	231.9	-0.137	-0.032	±0.052	-0.029	+0.056
A4	DBE glaciers	653.9	194.3	-0.286	-0.063	±0.058	-0.057	-0.396
A5	Sobral Peninsula	257.9	198.5	-0.173	-0.034	±0.018	-0.031	-0.145
A6	Cape Worsley coast	625.1	291.4	-0.742	-0.217	±0.051	-0.195	-0.800
A7	Drygalski Glacier	998.3	604.7	-3.187	-1.913	±0.074	-1.722	-2.179
	<i>Total</i>	<i>4245.3</i>	<i>2285.7</i>		<i>-2.646</i>	<i>±0.199</i>	<i>-2.382</i>	<i>-3.978</i>

742

743 **Table 2.** (a) Area extent of floating ice in 2016; (b) and (c) rate of surface elevation change and
 744 volume change 2013 to 2016 of floating ice (excluding the areas of frontal advance); (d) and (e)
 745 extent and volume of frontal advance (+) or retreat (-) areas.

ID	Basin name	(a) Floating area [km ²]	(b) Mean dh/dt [m a ⁻¹]	(c) Mean dV/dt [km ³ a ⁻¹]	(d) Advance/retreat area [km ²]	(e) Volume [km ³]
A2	Sjögren-Boydell	6.09	+1.250	0.062	+1.96	+0.403
A4	DBE glaciers	56.22	+0.131	0.060	+11.74	+2.017
A6	Cape Worsley coast	4.89	+0.194	0.008	+2.92	+0.550
A7	Drygalski Glacier	4.57	-2.231	-0.082	-1.40	-0.360

746



747 **Table 3.** Mean specific surface mass balance, b_n , for 2011 to 2016, and rates of surface mass
 748 balance (SMB), calving flux (CF) and mass balance by IOM (MB) in Gt a^{-1} for the periods 2011 to
 749 2013 and 2013 to 2016 for outlet glaciers north of Seal Nunataks.

ID	Glacier	b_n 11-16 $\text{kg m}^{-2} \text{a}^{-1}$	SMB 2011- 13 Gt a^{-1}	SMB 2013- 16 Gt a^{-1}	CF 2011- 13 Gt a^{-1}	CF 2013- 16 Gt a^{-1}	MB 2011 -13 Gt a^{-1}	MB 2013 -16 Gt a^{-1}
A2	SB	653	0.314	0.362	0.861	0.673	-0.547±0.144	-0.311±0.119
A3	APPE	903	0.446	0.470	0.517	0.488	-0.071±0.088	-0.018±0.089
A4	DBE	982	0.624	0.646	0.980	0.748	-0.356±0.181	-0.102±0.153
A7	Drygalski	1383	1.398	1.374	3.687	3.177	-2.289±0.619	-1.803±0.544

750 **Table 4.** Rate of surface elevation change for areas by means of TDM DEM differencing 2011 to
 751 2013 for glacier basins of the Larsen B embayment. dh/dt is the mean rate of elevation change of
 752 the area covered by the high resolution map (Fig. 5). The basin area refers to ice front positions
 753 delineated in TanDEM-X images of 2013-06-20 and 2013-07-01. The rates of ice volume change
 754 (dV/dt) and total mass balance (dM/dt) refer to grounded ice.

ID	Basin name	Total basin area [km^2]	TDM surveyed area [km^2]	Mean dh/dt [m a^{-1}]	dV/dt [$\text{km}^3 \text{a}^{-1}$]	Uncertainty [$\text{km}^3 \text{a}^{-1}$]	dM/dt [Gt a^{-1}]
B1	West of SN	638.1	494.1	-0.693	-0.342	±0.063	-0.308
B2	Hektoria Green	1167.5	491.8	-8.844	-4.312	±0.145	-3.881
B3	Evans	266.9	137.3	-2.700	-0.364	±0.032	-0.328
B4	Evans Headland	117.7	106.8	-0.476	-0.051	±0.011	-0.046
B5	Punchbowl	119.9	84.2	-0.761	-0.064	±0.013	-0.058
B6	Jorum	460.3	110.6	-2.157	-0.239	±0.063	-0.215
B7	Crane	1322.6	343.8	-2.318	-0.805	±0.179	-0.724
B8	Larsen B coast	142.6	95.8	-0.085	-0.046	±0.016	-0.041
B9	Mapple	155.4	92.4	-0.524	-0.048	±0.018	-0.043
B10	Melville	291.5	139.9	-0.859	-0.120	±0.036	-0.108
B11	Pequod	150.3	115.1	+0.025	+0.003	±0.015	+0.003
	<i>Total B1 to B11</i>	<i>4832.9</i>	<i>2211.6</i>		<i>-6.388</i>	<i>±0.495</i>	<i>-5.749</i>
B12	Rachel	51.8	38.9	-0.046	-0.002	±0.006	-0.002
B13	Starbuck	299.4	169.4	-0.118	-0.020	±0.035	-0.018
B14	Stubb	108.3	87.9	+0.116	-0.001	±0.011	-0.001
B15	SCAR IS coast	136.8	102.4	-0.184	-0.019	±0.014	-0.017
B16	Flask	1130.6	516.3	-0.629	-0.325	±0.138	-0.292
B17	Leppard	1851.0	946.5	-0.243	-0.230	±0.219	-0.207
	<i>Total B12 to B17</i>	<i>3577.9</i>	<i>1861.4</i>		<i>-0.597</i>	<i>±0.423</i>	<i>-0.537</i>



755 **Table 5.** Rate of surface elevation change for areas by means of TDM DEM differencing 2013 to
 756 2016 for glacier basins of the Larsen B embayment. dh/dt is the mean rate of elevation change of
 757 the area covered by the high resolution map (Fig. 6). The basin area refers to ice front positions
 758 delineated in TanDEM-X images of 2016-06-27 and 2016-08-01. The rates of ice volume change
 759 (dV/dt) and total mass balance (dM/dt) refer to grounded ice.

ID	Basin name	Total basin area [km ²]	TDM surveyed area [km ²]	Mean dh/dt [m a ⁻¹]	dV/dt [km ³ a ⁻¹]	Uncertainty [km ³ a ⁻¹]	dM/dt [Gt a ⁻¹]
B1	West of SN	638.7	485.6	-0.172	-0.084	±0.043	-0.076
B2	Hektoria Green	1215.7	552.8	-3.092	-1.708	±0.099	-1.538
B3	Evans	272.3	165.3	-1.494	-0.238	±0.021	-0.214
B4	Evans Headland	117.7	106.8	-0.331	-0.035	±0.007	-0.032
B5	Punchbowl	119.9	84.2	-0.488	-0.041	±0.009	-0.037
B6	Jorum	461.4	111.7	-0.989	-0.110	±0.042	-0.099
B7	Crane	1333.4	354.0	-0.753	-0.247	±0.120	-0.222
B8	Larsen B coast	142.6	96.0	-0.166	-0.016	±0.011	-0.014
B9	Mapple	155.4	92.8	-0.240	-0.022	±0.012	-0.020
B10	Melville	292.9	140.9	-0.584	-0.081	±0.024	-0.073
B11	Pequod	150.6	115.3	+0.069	0.008	±0.011	+0.007
	<i>Total B1 to B11</i>	<i>4900.2</i>	<i>2305.5</i>		<i>-2.574</i>	<i>±0.335</i>	<i>-2.318</i>
B12	Rachel	51.8	38.9	+0.040	0.002	±0.004	+0.002
B13	Starbuck	299.4	169.4	+0.006	0.001	±0.023	+0.001
B14	Stubb	108.3	87.9	+0.115	0.010	±0.007	+0.009
B15	SCAR IS coast	136.8	102.4	-0.087	-0.009	±0.009	-0.008
B16	Flask	1130.6	516.3	-0.604	-0.312	±0.092	-0.281
B17	Leppard	1851.0	946.5	-0.345	-0.337	±0.146	-0.303
	<i>Total B12 to B17</i>	<i>3577.9</i>	<i>1861.5</i>		<i>-0.645</i>	<i>±0.281</i>	<i>-0.580</i>

760

761

762



763 **Table 6.** (a) Area extent of floating ice in 2013 (A) and 2016 (B); (b) and (c) rate of surface
 764 elevation change and volume change 2011 to 2013 (A) and 2013 to 2016 (B) of floating ice
 765 (excluding the areas of frontal advance); (d) and (e) extent and volume of frontal advance areas.

ID	Basin name	(a) Floating area [km ²]	(b) Mean dh/dt [m a ⁻¹]	(c) Mean dV/dt [km ³ a ⁻¹]	(d) Advance area [km ²]	(e) Volume [km ³]
(A) 2011 - 2013						
B2	HG	19.81	-1.920	-0.308	31.65	11.676
B3	Evans	5.55	-1.264	-0.057	3.66	0.807
B6	Jorum	0.40	+3.510	+0.011	0.54	0.134
B7	Crane	2.01	+3.770	+0.061	4.96	2.164
(B) 2013 - 2016						
B2	HG	62.09	-0.002	-0.001	47.96	11.270
B3	Evans	14.56	-0.652	-0.077	5.39	0.931
B6	Jorum	1.15	+0.305	+0.003	0.78	0.165
B7	Crane	7.99	-2.620	-0.169	10.54	3.301
B10	Melville	0.88	-0.966	-0.007	1.20	0.219

766

767 **Table 7.** Mean specific surface mass balance (b_n) 2011-2016, annual surface mass balance (SMB)
 768 and calving flux (CF) 2011-2013 and 2013-2016, and resulting IOM mass balance (MB) in Gt a⁻¹
 769 for Larsen B glaciers.

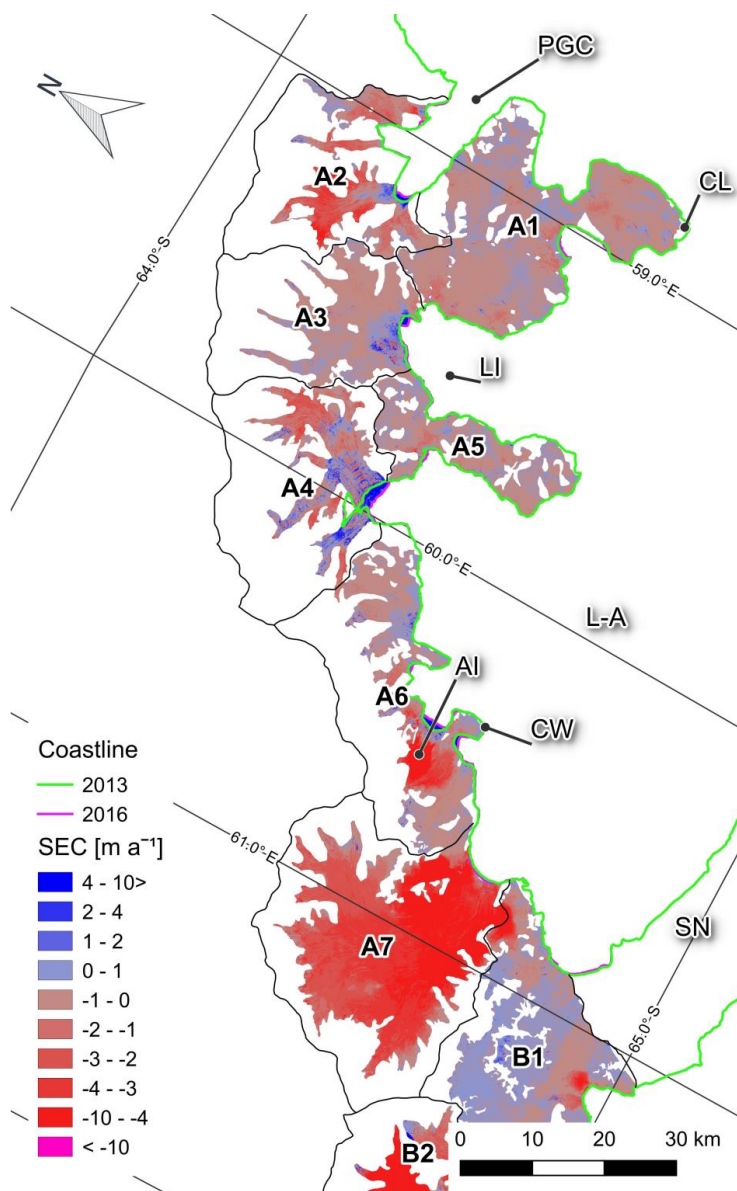
ID	Glacier	b_n 11-16 kg m ⁻² a ⁻¹	SMB 2011- 13 Gt a ⁻¹	SMB 2013- 16 Gt a ⁻¹	CF 2011- 13 Gt a ⁻¹	CF 2013- 16 Gt a ⁻¹	MB 2011 -13 Gt a ⁻¹	MB 2013 -16 Gt a ⁻¹
B2	HG	1400	1.563	1.644	5.733	3.389	-4.170±0.936	-1.745±0.590
B3	Evans	562	0.137	0.156	0.389	0.304	-0.252±0.065	-0.148±0.053
B6	Jorum	884	0.376	0.427	0.457	0.361	-0.081±0.092	+0.066±0.86
B7	Crane	837	1.023	1.159	2.093	1.565	-1.070±0.280	-0.406±0.247
B10	Melville	330	0.091	0.100	0.146	0.144	-0.055±0.021	-0.044±0.022
B13	Starbuck	287	0.078	0.091	0.067	0.068	+0.011±0.014	+0.023±0.016
B16	Flask	693	0.722	0.824	1.085	1.118	-0.363±0.163	-0.294±0.176
B17	Leppard	500	0.874	0.961	1.760	1.780	-0.886±0.237	-0.819±0.246

770

771



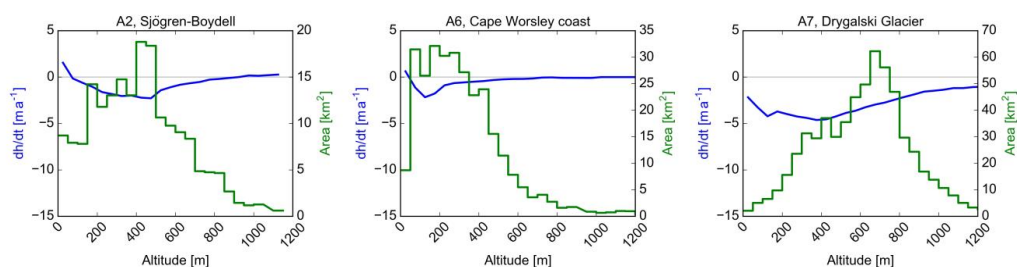
772 **Figures**



773

774 **Figure 1.** Map of surface elevation change dh/dt (m a^{-1}) June/July 2013 to July/August 2016 on
775 glaciers north of Seal Nunataks (SN). AI – Arrol Icefall, CL – Cape Longing, CW – Cape Worsley,
776 L-A – Larsen A embayment, LI – Larsen Inlet, PGC – Prince-Gustav-Channel.

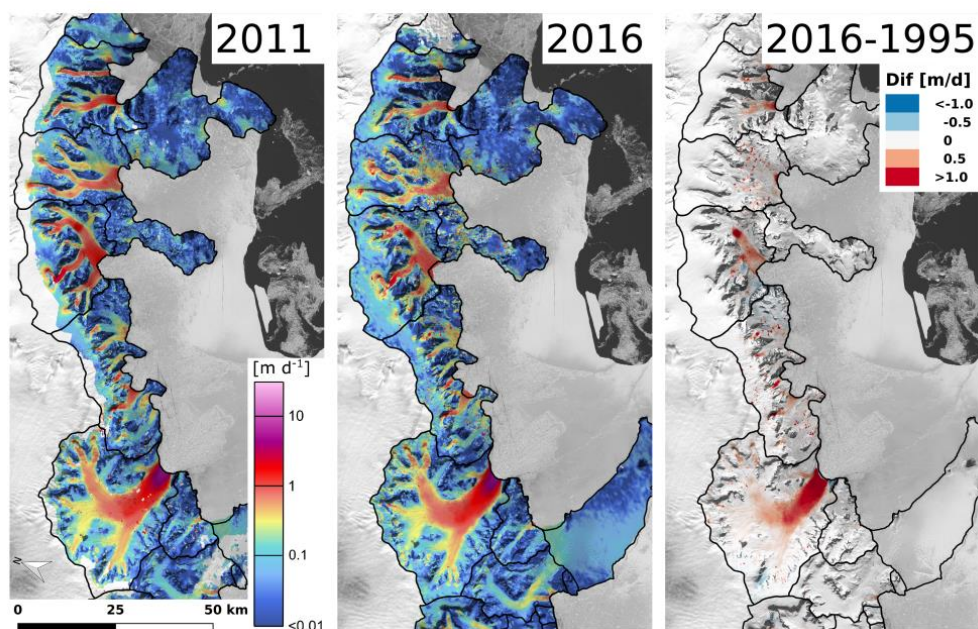
777



778

779 **Figure 2.** Rate of glacier surface elevation change dh/dt (in $m a^{-1}$) 2013 to 2016 versus altitude in
 780 50 m intervals for basins A2, A6 and A7. Green line: hypsometry of surveyed glacier area in km^2 .

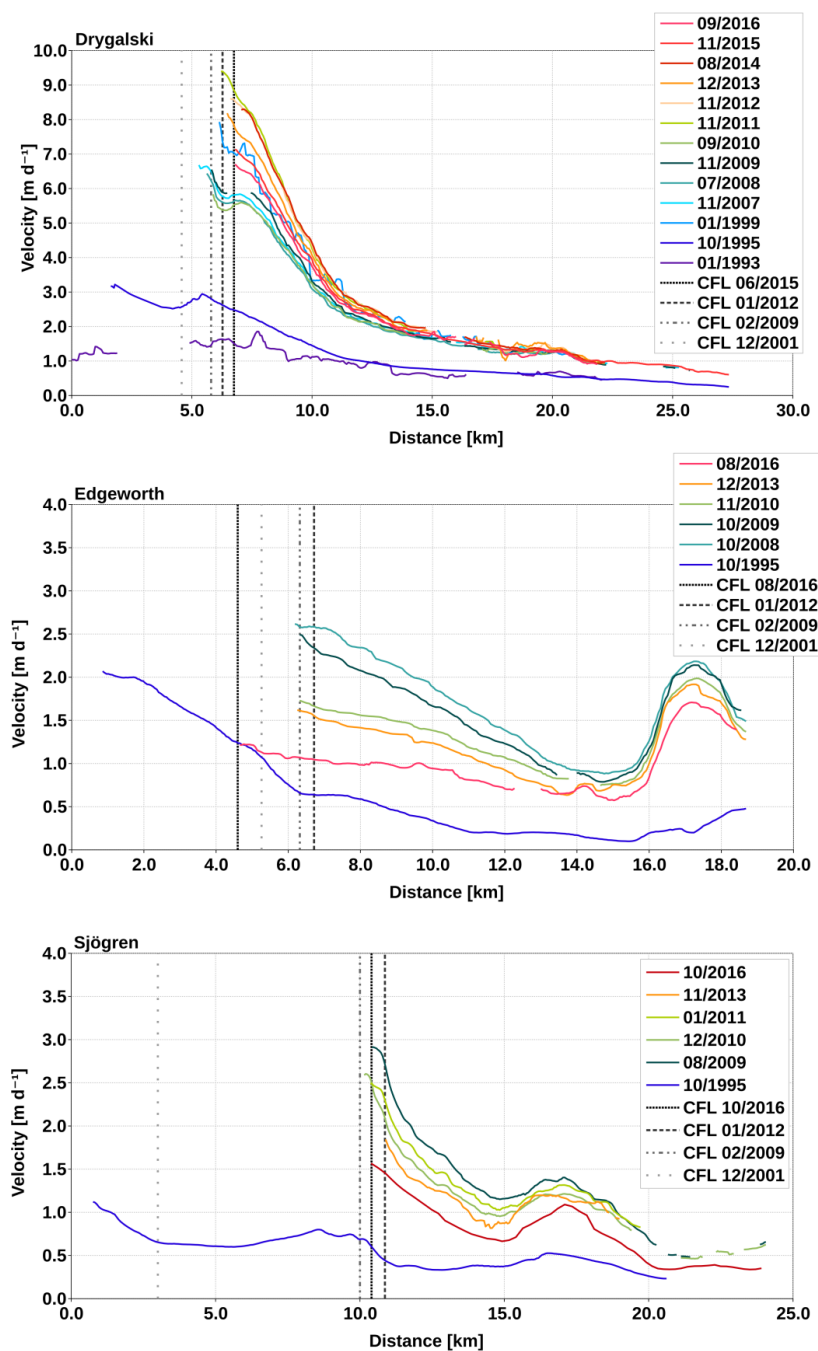
781



782

783 **Figure 3.** Magnitude of ice velocity [$m d^{-1}$] 2011 and 2016 derived from TerraSAR-X and
 784 TanDEM-X data. Gaps in 2011 filled with PALSAR data and in 2016 filled with Sentinel-1 data.
 785 Right: Map of velocity difference 2016 minus 1995 (November).

786

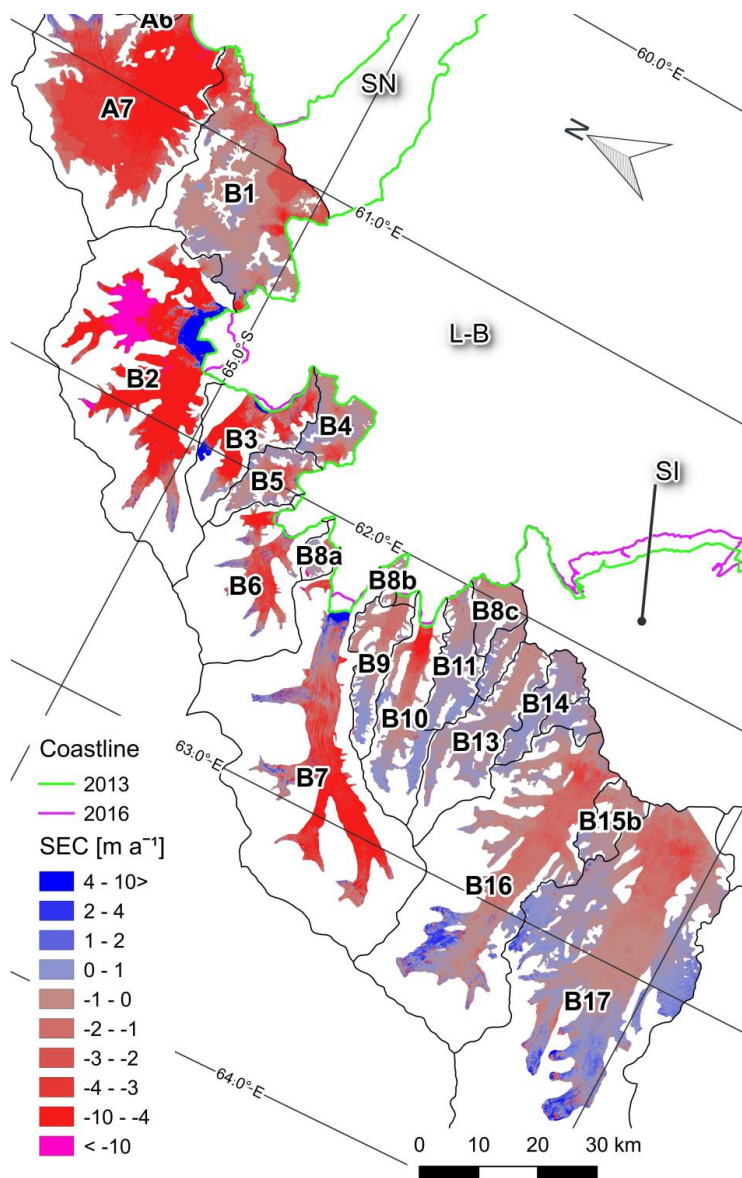


787

788 **Figure 4.** Surface velocities along the central flow lines of Drygalski, Edgeworth and Sjögren
 789 glaciers and their frontal positions on different dates (month/year). The x- and y-scales are different
 790 for individual glaciers. Vertical lines show positions of the calving front.

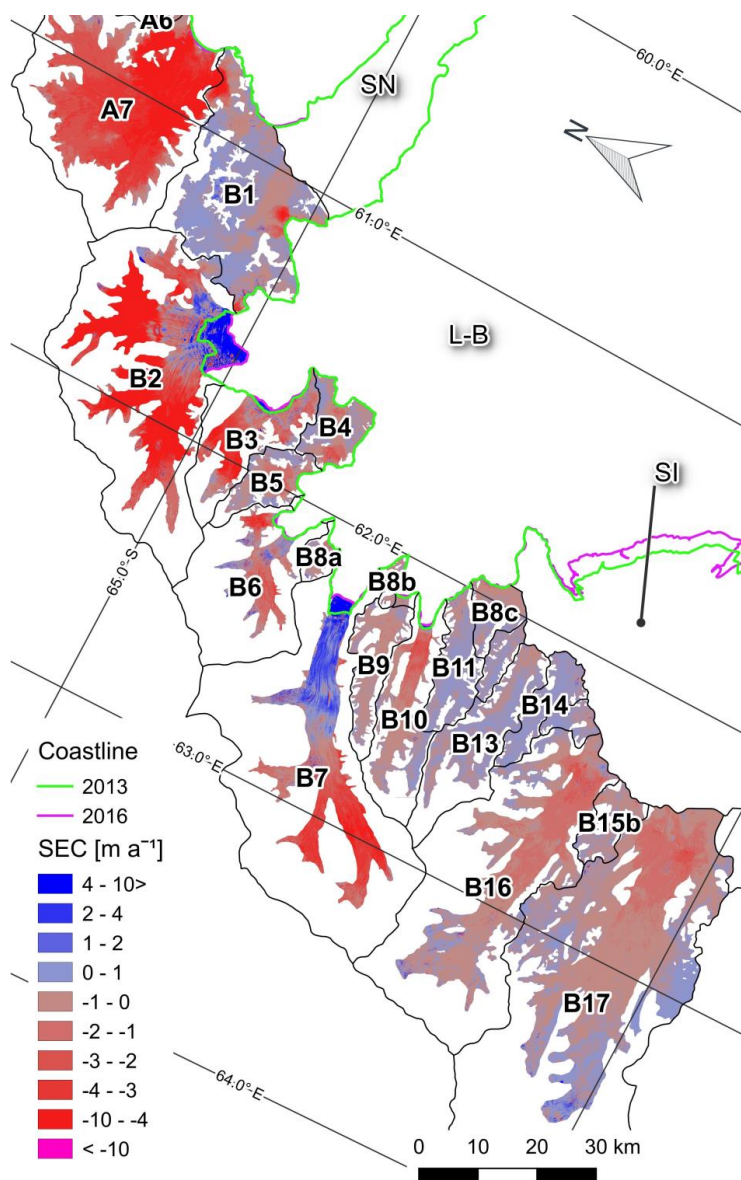


791



792

793 **Figure 5.** Map of surface elevation change (SEC m a^{-1}) May/June 2011 to June/July 2013 on
 794 glaciers of Larsen B embayment (L-B). SN – Seal Nunataks. SI -SCAR Inlet ice shelf.



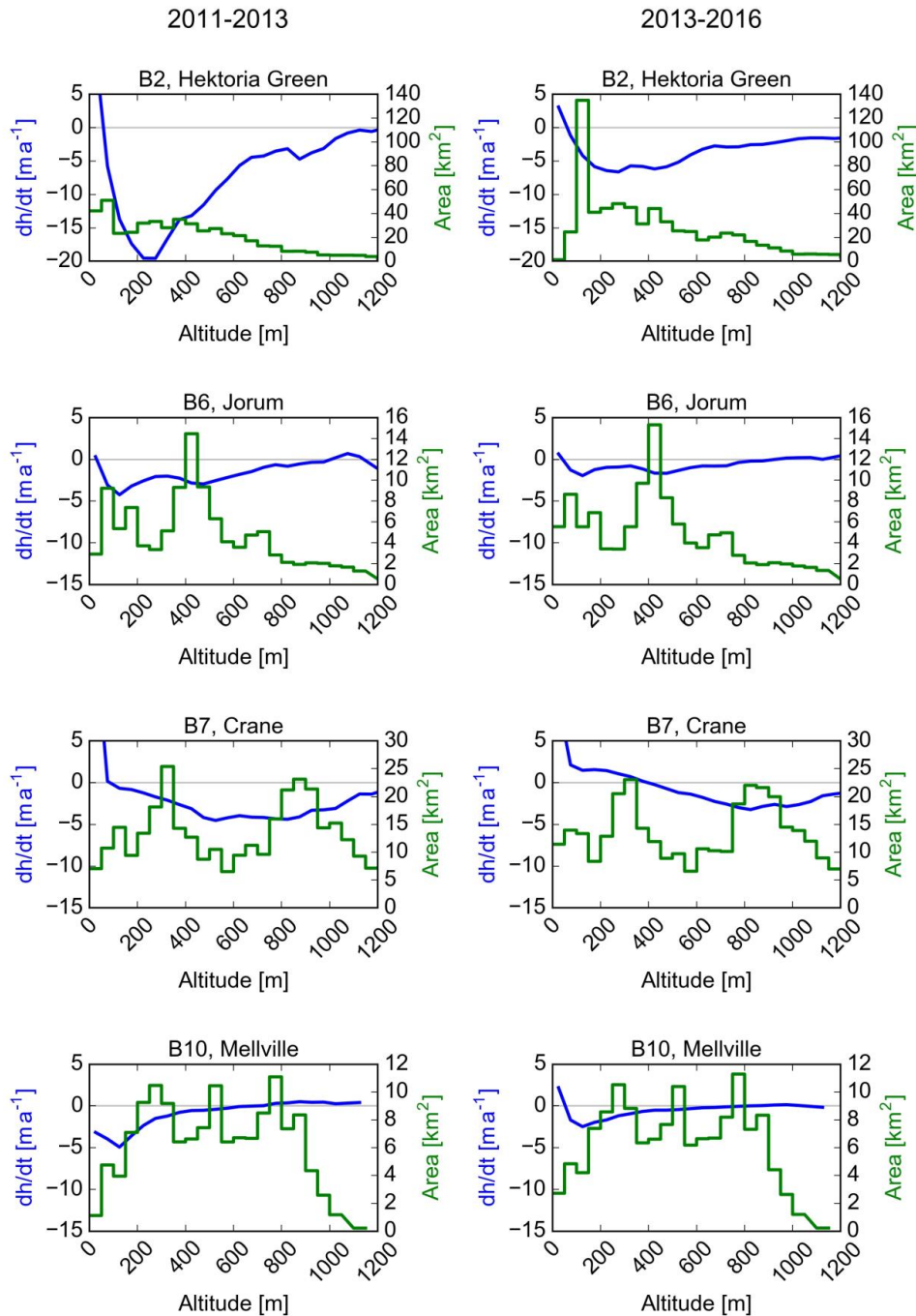
795

796 **Figure 6.** Map of surface elevation change (SEC m a^{-1}) June/July 2013 to July/August 2016 on
797 glaciers of Larsen B embayment (L-B). SN – Seal Nunataks. SI -SCAR Inlet ice shelf.

798

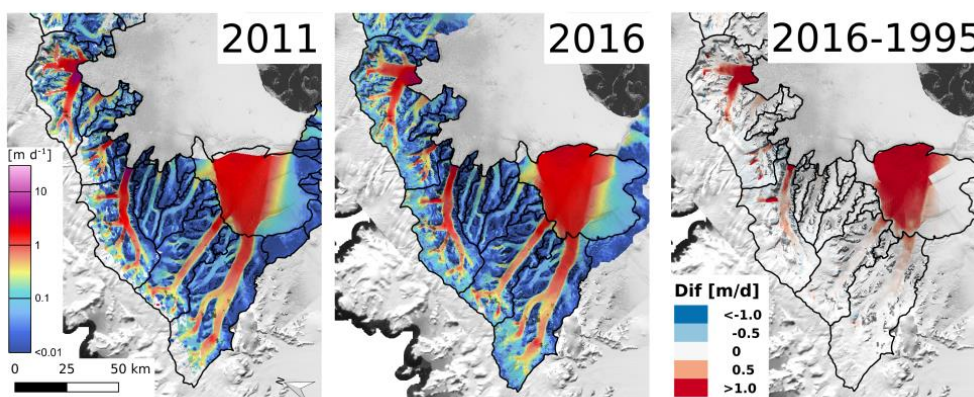
799

800



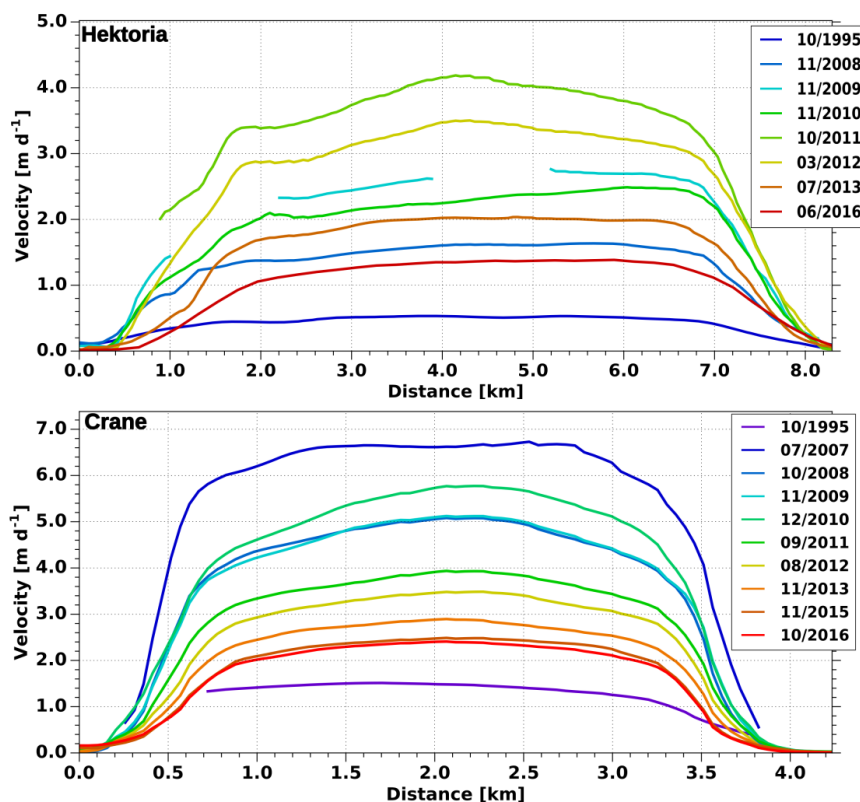
801

802 **Figure 7.** Rate of glacier surface elevation change dh/dt (in $m a^{-1}$) 2011 to 2013 and 2013 to 2016
 803 versus altitude in 50 m intervals for basins B2, B6, B7 and B10. Green line: hypsometry of
 804 surveyed glacier area in km^2 .



805

806 **Figure 8.** Magnitude of ice velocity [m d^{-1}] 2011 and 2016 derived from TerraSAR-X and
 807 TanDEM-X data. Gaps in 2011 filled with PALSAR data and in 2016 filled with Sentinel-1 data.
 808 Right: Map of velocity difference 2016 minus 1995.



809

810 **Figure 9.** Surface velocity across the flux gate of Hektor Glacier and Crane Glacier on different
 811 dates (month/year) between 1995 and 2016.